4 Plasma Performance Assessment

4.1 Introduction

ITER will be the first fusion device with significant Q (the ratio of fusion power to additional heating power) and extended burn. ITER is designed as an experimental device with extensive diagnostics and a considerable flexibility in fusion power, plasma density, beta, shaping, heating and current drive, fuelling methods, and replaceable in-vessel components. This

flexibility has been deemed essential for accommodating uncertainty in projection, and for investigating and optimising the burning plasmas well as to facilitate the exploration of new operation regimes attractive for a reactor. The principal physics goals of ITER are:

(i) to achieve extended burn in inductively-driven plasmas with Q of at least 10 for a range of operating scenarios and with a duration sufficient to achieve stationary conditions on the time scales characteristic of plasma processes;

(ii) to aim at demonstrating steady-state operation using non-inductive current drive with a ratio of fusion power to input power for current drive of at least 5.

In addition, the possibility of higher Q operation will be explored if favourable confinement conditions can be achieved.

The reference plasma operating scenario for ITER inductive operation is the ELMy H mode, which has been observed reliably and reproducibly in many tokamaks. Furthermore, the properties of H-mode have been investigated over the last 18 years, establishing the scaling laws for projection. The rules and methodologies for projection of plasma performance to the ITER scale are basically those established in the ITER Physics Basis (IPB)[1]. After completion of the IPB document, continued physics R&D has yielded new results, which are reflected in the present analyses.

The key physics issues relating to plasma performance in the ELMy H-mode regime are the following:

- H-mode confinement at sufficiently high density and beta to produce the requisite fusion power, and hence Q value,
- power and particle exhaust to ensure acceptable levels of helium, plasma impurities and heat load on the divertor target,
- small losses of α-particles via TF ripple or collective instabilities, to enable efficient transfer of α-particle energy to the thermal plasma and to prevent damage to the plasma-facing components,
- global magnetohydrodynamic (mhd) stability and plasma control capability to reduce heat and/or electromagnetic loads due to disruptions and ELMs to ensure adequate life time of the in-vessel components.

The development of plasma operation scenarios that exploit active profile control to access enhanced confinement regimes with an internal transport barrier (ITB), which has occurred in the course of the EDA, has allowed greater emphasis to be placed on the use of such scenarios in ITER. In particular, these regimes offer the prospect of establishing reactor-relevant, steady state operation in which a significant fraction of the plasma current is generated via the bootstrap effect. Although the precise conditions for the development of ITBs are uncertain, the aim has been to provide ITER with the necessary plasma control tools to facilitate access to such modes of operation. Flexibility in the ITER design through plasma shaping, a mixture of heating and current drive systems, and availability of techniques for suppression of

[1] ITER Physics Expert Groups et al., ITER Physics Basis, Nucl. Fusion 39 (1999) 2137

neoclassical tearing modes (NTMs) and resistive wall modes (RWMs), favours the exploitation of plasma scenarios with either shallow monotonic or negative central shear. Sophisticated diagnostics of key profiles such as q, pressure, and rotation will be required to operate with a high level of reliability from the first phase of plasma experiments, and this has been acknowledged in assigning measurement priorities. The question of α-particle losses, via TF ripple, is anticipated to be particularly pronounced in these regimes, and the design of the ferromagnetic inserts reflects this consideration. It is also possible that collective instabilities, e.g. TAE modes, are excited in these regimes, but these instabilities are expected to be tolerable in scenarios with flat or weakly inverted q profiles. High-field-side pellet injection would create a significant density gradient in the far off-axis zone, which is shown to be essential for reducing or eliminating the need for far off-axis current drive. Predictions of steady-state operation in ITER, therefore, build upon these recent developments and reflect the expectation that considerable further progress can be achieved in the fusion programme in the future to resolve remaining uncertainties.

This section presents the analysis results on plasma performance, control and operation. In subsection 4.2, the bases of performance analysis are summarised. In subsection 4.3, plasma operation scenarios are described for inductive, hybrid and steady-state operation. Subsection 4.4 presents the analysis results of plasma performance. Operation boundaries, sensitivity to assumptions, high-Q, and ignition operation, are assessed. Also discussed are the projections of hybrid and steady-state operation, and the requirements for current drive for steady state. The performance projection of the divertor pedestal and ELMs is presented and assessed in subsection 4.5. Subsection 4.6 deals with energetic particle confinement issues, i.e. TAE modes and ripple losses. Subsection 4.7 elaborates the conclusions.

4.2 Performance Analysis Basis

In this subsection, the basis of performance analysis is summarised.

4.2.1 Global Scaling Expression for the Thermal Energy Confinement Time

The thermal energy confinement time of ELMy H-mode, the reference confinement regime for inductive Q = 10 operation, is described by the ITERH-98P(y,2) empirical scaling as

$$\tau_{E,th}^{IPB98(y,2)} = 0.0562 H_{H98(y,2)} I_p^{0.93} B_T^{0.15} \bar{n}_e^{0.41} P^{-0.69} R^{1.97} M^{0.19} \kappa_a^{0.78} \varepsilon^{0.58} \qquad (4.2.1\text{-}1)$$

where the units are s, MA, T, 10^{19}m^{-3}, MW, m, and amu, respectively, $\varepsilon = a/R$, and the elongation κ_a is defined as $\kappa_a = V/(2\pi^2 R a^2)$ with V being the plasma volume. $H_{H98(y,2)}$ denotes a constant normally taken to be unity but varying here between 0.85 and 1.15 in order to assess the sensitivity of the machine performance to energy confinement changes.

4.2.2 Radiation Correction for the Energy Confinement Time

The power P used for scaling derivation is the total heating power with the deduction of

power lost through the charge exchange and unconfined ion orbits only[1]. No correction for radiation losses was applied. In ITER, the fraction of the input power lost by radiation is estimated to be more than 30%. The numerical simulations for ITER have led to the following radiation loss account in the expression for the net heating power:

$$P = P_{\alpha} + P_{oh} + P_{add} - (P_{brem} + P_{cycl} + P_{line}/3), \qquad (4.2.2\text{-}1)$$

where P_{α} is the α-particle power, P_{oh} the ohmic power, P_{add} the additional heating power, P_{brem} the bremssrtahlung power, P_{cycl} the cyclotron radiation power, and P_{line} the line radiation power.

4.2.3 Temperature and Density Profiles

The temperature and density profiles are estimated using 1.5D transport codes, PRETOR and ASTRA. There are two approaches to calculate the radial dependencies of transport coefficients. It is possible to use the radial dependencies from any specific model[2] or to use formal dependencies such as D and $\chi \sim \gamma_1(1 + \gamma_2 (\rho/\rho_{edge})^2)$ with $\gamma_2 \sim 3$ similar to many experiments[4], and a normalisation factor γ_1 chosen to fit the scaling law for τ_E. The formal approach assumes also some relations, based on the experimental background[3] $\chi_i/\chi_e = 2$, $\chi_i/\chi_\varphi = 1$, $D_e/\chi_e = 1$, where χ_φ is momentum diffusivity. For helium diffusion, both $D_{He} = \chi_i$, or $D_{He} = \chi_e$ are assumed.

4.2.4 Additional Heating and Current Drive

For nominal operation, the additional heating power of 40 MW is made up of 33 MW of NB and 7 MW of RF heating.

In 1.5D transport simulations using the PRETOR code[3], the RF power is assumed to be deposited in the core region (normalised minor radius $r/a < 0.3$), with 50% of the power heating the ions and 50% the electrons. For more detailed analysis, the RF power deposition profile and ion heating fraction can be obtained numerically, for example by coupling with the PION ICH&CD simulation code[4]. For sensitivity analyses, the ion heating fraction is varied as a parameter. The normalised current drive efficiency ($\gamma_{CD} = I_{CD}\langle n_e\rangle R/P_{CD}$) for RF is also an input parameter. A typical case for ECCD has $\gamma_{CD} = 0.3\times10^{20}AW^{-1}m^{-2}$ for on-axis current drive and $\gamma_{CD} = 0.1\times10^{20}AW^{-1}m^{-2}$ for current drive in the periphery.

In the ASTRA code[5], the ECCD efficiency and absorption width are calculated by approximate formulae obtained using the OGRAY[6] code, in which ray tracing and Fokker-Planck equations are solved for the fast electrons. For the case of LHH&CD, the driven

[1] K. Thomsen, D.J. Campbell, J.G. Cordey, et al., Nucl. Fusion **34** (1994) 131
[2] ITER Physics Basis, Nucl. Fus. **39** (1999) 2225-2228
[3] D. Boucher, et. al., in Proc. 16th IAEA Fusion Energy Conference, Montreal, 1996 (IAEA,Vienna, 1997) 945
[4] V. Bergeaud, L.-G. Eriksson, D.F.H. Start, Nucl. Fusion 40 (2000) 35
[5] G.V. Pereverzev, et. al., IPP 5/42 (1991)
[6] A.V. Zvonkov, A. Yu. Kuyanov, A.A. Skovoroda, and A.V. Timofeev, Plasma Phys. Rep., 24 (1998) 389

current profile is prescribed and γ_{CD} is assumed to be $0.3\times10^{20}AW^{-1}m^{-2}$ in the peripheral region.

NB injection in the ASTRA code is calculated using a Fokker-Planck solver taking account of shape of power distribution within the beam footprint, multi-step ionisation cross sections, orbital losses and neo-classical effects[1]. In the PRETOR code, the NB power deposition profile is calculated with a pencil beam assumption and the current-drive efficiency is given with the Mikkelsen-Singer approximation[2]. The ACCOME code is used for detailed analysis and verification of the PRETOR calculation. The injection energy is 1 MeV, and the injection radius and height are varied within the available design range.

4.2.5 Helium Contamination and Impurities

The simplest models used for the ITER predictive simulations consider a reduced set of one-dimensional fluid-like equations, which represent the evolution of plasma density, momentum and energy for each of the plasma species[3]. In the reduced version, the charged particle density transport is simulated only for the electron and helium components n_e and n_{He}. For the other impurity species, the fractions of the electron density $n_{zk} = f_k n_e$, are assumed and the fuel densities n_D, n_T are calculated from the quasi-neutrality condition: $n_e=n_D+n_T+2n_{He}+\Sigma_k Z_k n_{zk}$. The electron source S_e is defined from pellet injection and/or from edge neutral fuelling modelling. The helium source S_{He} is defined from fusion reaction calculations. An alternative version of this approach is an n_D, n_T transport simulation with n_e calculated from quasineutrality. The impurity charge Z_k is determined from a coronal equilibrium model[4]. The momentum transport is considered only for the toroidal component. The heat transport description is reduced to the electron heat transport equation with T_e, n_e, and a summarised ion heat transport equation with T_i, $n_I = n_D+n_T+n_{He}+\Sigma_k n_{zk}$, since all ion species have the same temperature on the transport time scale.

4.2.6 Divertor

Divertor modelling is carried out with the B2-Eirene code[5]. This package consists of a two-dimensional, multi-fluid model for the DT and impurity ions and electrons coupled to a Monte-Carlo model for the neutral particles. The main physical assumptions used in the B2-Eirene code package are described in the ITER Physics Basis[6].

[1] A.R. Polevoi, H. Shirai and T. Takizuka, JAERI Data/Code 97-014
[2] D.R. Mikkelsen and C.E. Singer, Nucl. Technol. /Fusion **4**, 237 (1983)
[3] ITER Physics Basis, Nucl. Fus. **39** (1999) 2178-2184
[4] D.E. Post, et al., Atomic Data and Nuclear Data Tables, **20** (1977) 397
[5] D. Reiter, et al., Plasma Phys. Contr. Fusion **33** (1991) 1579; R. Schneider, et al., J. Nucl. Mater, **196–198** (1992) 810
[6] ITER Physic Basis. Chapter 4: Power and Particle Control, Nucl. Fusion, **39** (1999) 2391

4.2.7 Beta Limit

Ideal MHD alone constitutes the basis for the experimental observation that kink and/or ballooning instability onset develops in most cases for $3 \leq \beta_N \leq 4$ (i.e. at ideal MHD limit) or for $\beta_N > 4l_i$ (the wall-at-infinity limit).

Neo-classical tearing modes (NTMs) pose a potential challenge to ITER operation. If NTMs are triggered and uncontrolled in ITER, they will likely limit the attainable normalised β to values of β_N <2.

In some steady state scenarios, the minimum safety factor can be made above 2, thus eliminating the possibility of tearing modes of (m,n) = (2,1) and (3,2).

4.2.8 Plasma Density

For ITER, two distinct density-limiting processes observed in present tokamaks are relevant, namely a disruptive limit, and a performance limit causing a confinement degradation in H-mode and ultimately a return to L-mode confinement. The disruptive empirical limit is usually (but not inevitably) characterised by $n_{max} \sim n_G$, (Greenwald density n_G $[10^{20}\,m^{-3}] = I[MA]/\pi a^2[m]$). The fraction of Greenwald density where the performance limit sets in is also dependent on the triangularity and on the onset condition for Type II ELMs. In the performance calculations here it was characterised by the H-L back-transition based on the H-mode power threshold scaling and is described in the next section.

4.2.9 L to H-Mode Power Threshold

The recommended form for the H-mode power threshold empirical scaling[1] is

$$P_{L\text{-}H} = 2.84 M^{-1} B_T^{0.82} \bar{n}_e^{0.58} R^{1.00} a^{0.81} \quad \text{(rms err. 0.268)} \qquad (4.2.9\text{-}1)$$

in MW, amu, T, 10^{20} m^{-3} and m, respectively, with M being the effective isotopic mass of the plasma fuel. This scaling expression is based on the latest version of the threshold database (DB3) including results from recent dedicated H-mode threshold experiments in Alcator C-Mod and JT–60U, the latter using the new 'W' shaped divertor. For ITER-like devices, this scaling yields an H-mode power threshold prediction which is approximately a factor of 2 lower than that predicted by an earlier version[2]. $P_{L\text{-}H}$ is defined as the total input power in the threshold database. In ITER analyses $P_{L\text{-}H}$ is calculated by Eq. (4.2.2-1), which gives an about 30% more conservative value.

[1] J.A. Snipes et al., Plasma Phys. Control. Fusion **42** (2000) A299-A308
[2] ITER Physics Basis, Chapter 2 Section 4.3 (Eq. (5) in Table 2), Nucl. Fusion **39** (1999) 2196

4.3 Plasma Operation Scenarios

4.3.1 Inductive Operation Scenarios

The time evolution of plasma parameters is investigated by the 1.5D transport codes PRETOR[1] and ASTRA[2]. Here, the plasma shape is fixed during the simulation and the 2D equilibrium is re-computed if the pressure change exceeds a given value. The PF coil system is consistent with the scenarios throughout the whole phase of the plasma operation. Time histories of plasma parameters such as plasma current (I_P), electron density (n_e), electron and ion temperature (T_e, T_i), heating power by NB (P_{NB}), heating power by RF (P_{RF}), safety factor at 95% flux surface (q_{95}), safety factor at the magnetic axis (q_0) and fusion power (P_{FUS}) are calculated.

Figure 4.3.1-1 shows the time evolution of plasma parameters in a typical operation scenario with the flat-top current of 15 MA. The simulation is performed from the X-point formation (XPF) to the end of burn (EOB). Plasma heating starts just after the current flat top. At this time, the electron density should be small enough to keep the threshold power (P_{LH}) for L-H transition low and large enough to avoid shine-through of neutral beams. In this case, NB heating (16.5 MW, 1 MeV) starts at 100 s when $\langle n_e \rangle = 4\times10^{19} m^{-3}$. In the simulation, the H-mode transition occurs at 110 s when the second NB is started and the total NB power increases to 33 MW. During the flat top phase, 33 MW of NB and 7 MW of RF heating are used and about 400 MW of fusion power is produced (Q = 10). 2% impurity of beryllium is assumed and the helium accumulation is calculated for the pumping speed which provides $\tau_{He}^*/\tau_E = 5$.

[1] D. Boucher, et al., in Proc. 16th IAEA Fusion Energy Conference, Montreal, 1996 (IAEA,Vienna, 1997) 945
[2] G.V. Pereverzev, et al., IPP 5/42 (1991)

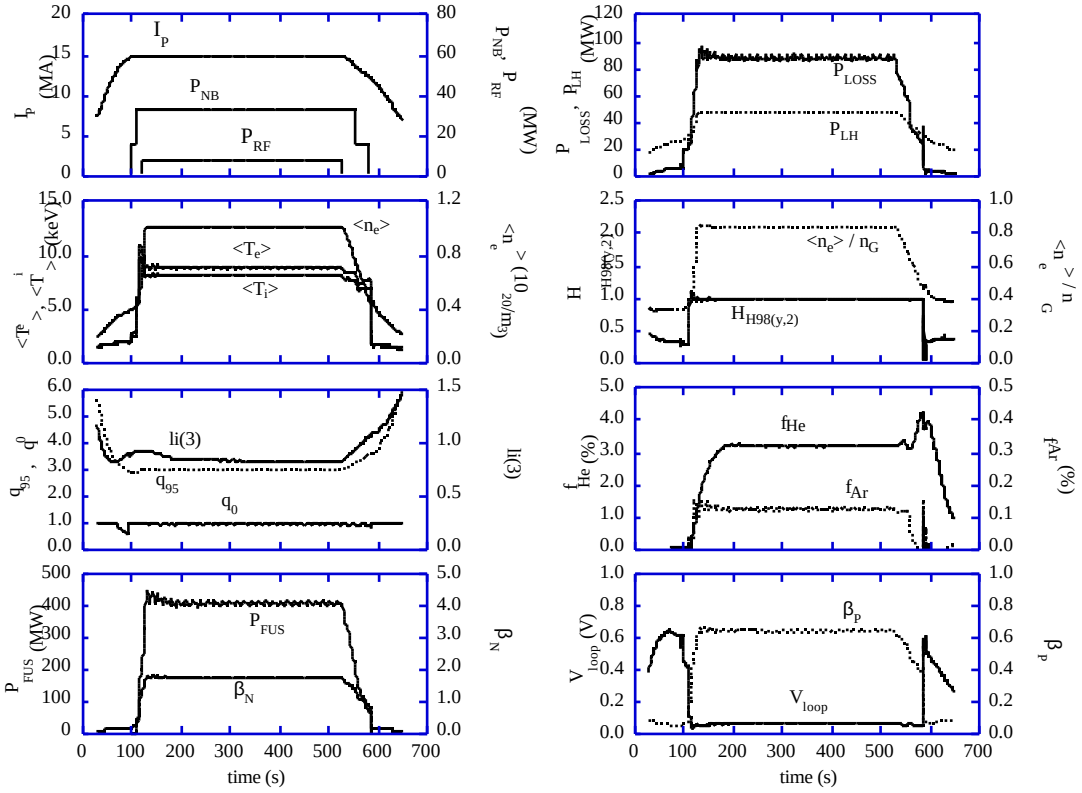

Figure 4.3.1-1 Time Evolution of Plasma Parameters

Here, plasma current (I_P), neutral beam heating power (P_{NB}), RF heating power (P_{RF}), volume-averaged electron density ($<n_e>$), electron and ion temperatures ($<T_{e,i}>$), safety factor at 95% flux surface (q_{95}), safety factor at the magnetic axis (q_0), internal inductance ($l_i(3)$), fusion power (P_{FUS}), normalised beta (β_N), loss power (P_{LOSS}), L-H transition threshold power (P_{L-H}), Greenwald parameter ($<n_e>/n_G$), HH-factor ($H_{H98(y,2)}$), average helium fraction (f_{He}), argon fraction (f_{Ar}), loop voltage (V_{loop}), and poloidal beta (β_P) are shown.

Argon impurity up to 0.12% is seeded. The necessary seeding fraction is calculated on the basis of a simplified divertor model[1] to keep the power to the divertor region at a conservatively low value, i.e., about 30 MW, which gives less than 5 MW/m^2 on the divertor target. In this example, additional 37 % is radiated outside the separatrix and the total heat load to the divertor target is 30 MW. However, the allowable heat load is 60 MW on the divertor target, therefore, the minimum requirement for the radiation cooling outside the separatrix is 13 %.

The corresponding effective charge (Z_{eff}) of 1.66 and a helium contribution of about 0.16 with f_{He}(axis) = 4.3% are obtained. The power P_{LOSS} across the pedestal top is 87 MW (the power P_{SOL} across the separatrix flux surface is about 75 MW). This power and a separatrix density of 3×10^{19}m^{-3} are taken as input for a 2D divertor simulation code and are shown to be consistent with acceptable divertor conditions[2], where the separatrix density of 3×10^{19}m^{-3} is assumed as a conservative estimate. The loop voltage at the flat top is about 75 mV and the burn time is estimated to be 400 s with an available flux of 30 Vs. To come to the final plasma

[1] M. Sugihara, et al., 12th PSI Conference in Controlled Fusion Devices, St. Raphael (1996)
[2] A. Kukushkin, et al., 14th PSI Conference, Rosenheim (2000)

shutdown, the transition to L mode occurs at 580 s, when all the heating power is switched off. The main physics parameters during flat top for both 400 MW and 500 MW operation scenarios are summarised in Table 4.3.1-1.

Table 4.3.1-1 Parameters of ITER Inductive Operation Scenarios

Parameter	400 MW	500 MW
R/a (m/m)	6.2/2.0	6.2/2.0
Volume (m^3)	831	831
Surface (m^2)	683	683
Sep.length (m)	18.2	18.2
$S_{cross\text{-}sect.}$ (m^2)	21.9	21.9
B_T (T)	5.3	5.3
I_P (MA)	15.0	15.0
κ_X/δ_X	1.85/0.48	1.85/0.48
κ_{95}/δ_{95}	1.70/0.33	1.70/0.33
l_i (3)	0.84	0.84
V_{loop} (mV)	75	75
q_{95}	3	3
β_N	1.8	2.0
$<n_e>$ (10^{19} m^{-3})	10.1	11.3
$<n_e>/n_G$	0.85	0.94
$<T_e>$ (keV)	8.8	8.9
$<T_i>$ (keV)	8.0	8.1
$<\beta_T>$ (%)	2.5	2.8
β_p	0.65	0.72

Parameter	400 MW	500 MW
$P_{RF} + P_{NB}$ (MW)	7 + 33	17 + 33
P_{OH} (MW)	1	1
P_{TOT} (MW)	121	151
P_{BRM} (MW)	21	26
P_{SYN} (MW)	8	8
P_{LINE} (MW)	18	27
P_{RAD} (MW)	47	61
P_{FUS} (MW)	400	500
$P_{LOSS}/P_{L\text{-}H}$	87/48	104/51
Q	10	10
τ_E (s)	3.7	3.4
W_{th} (MJ)	320	353
W_{fast} (MJ)	32	34
$H_{H98\ (y,2)}$	1.0	1.0
τ_{He}^*/τ_E	5	5
$Z_{eff,\ ave}$	1.66	1.72
$f_{He,axis\ /\ ave}$ (%)	4.3/3.2	4.4/3.2
$f_{Be,axis}$ (%)	2.0	2.0
$f_{Ar,axis}$ (%)	0.12	0.14

4.3.2 Hybrid Operation Scenario

A hybrid mode of operation, in which a substantial fraction of the plasma current is driven by non-inductive current drive power and the bootstrap current, is a promising route towards the establishment of true steady-state modes of operation. Operation longer than 1,000 s with Q = 5 is investigated with current drive power up to 100 MW and a modest requirement on confinement ($H_{H98(y,2)}$ = 1.0). In this section, the burn time of hybrid mode operation is estimated. In order to optimise the plasma parameters such as plasma current, a simple formula[1] is used for the estimation of flux available for the burning. Current-drive efficiency of NB injection is given by the Mikkelsen-Singer approximation[2] and the normalised current drive efficiency for RF is fixed to $0.3\times10^{20}AW^{-1}m^{-2}$. A Gaussian-type RF power deposition profile in the core (normalised minor radius r/a < 0.3), with 50% to ions and 50% to electrons, is assumed. The NB current drive efficiency was verified by the ACCOME code.

[1] Y. Murakami and M. Sugihara, Fusion Technology, **24**, (1993) 375
[2] D.R. Mikkelsen and C.E. Singer, Nucl. Technol., Fusion **4**, (1983) 237

Figure 4.3.2-1 shows the achievable burn duration as a function of fusion gain Q. Here, 0D modelling is used and the plasma current is optimised under the condition that the maximum normalised beta β_N and the ratio $<n_e>/n_G$ of electron density to Greenwald density are given. It is seen from Figure 4.3.2-1 that the maximum burn time for operation with Q = 10 is about 500 s when full size plasma (R/a = 6.2 m/2.0 m) is adopted. In this case, I_P = 14.2 MA and P_{FUS} = 320 MW for the flat density profile. Operation with Q > 10 is possible with a limited burn time. The burn time increases with decreasing Q and I_p. It is seen that operation with burn time of 1000 s is possible when Q = 5. In the low-Q region (Q < 10), the burn time can be prolonged by adopting a plasma with a smaller minor radius (R/a = 6.35 m/1.85 m). The achievable burn time is about 1300 s when Q = 5, β_N = 2.0 and $<n_e>/n_G$ = 0.85. In this case, the fusion power is 350 MW, and the current drive power is 70 MW. (The fusion power depends on the plasma profiles). If β_N can be increased to 2.5, the expected burn time becomes longer than 2000 s. In the high-Q region, the burn time is not sensitive to β_N but can be prolonged by increasing the operating density. The burn time can be prolonged further if the flux Ψ_{HEAT} used for heating (10 Vs) at the plasma current flat top is reduced by heating the plasma before the flat top.

1.5D transport simulation is also done for the hybrid operation. The results are shown in Table 4.3.2-1 (#1 ~ #4). All of these scenarios satisfy Q ≥ 5 and a burn time ≥ 1000 s at $H_{H98(y,2)}$ = 1.0. The scenarios #1 and #3 are compatible with the additional heating power available in the initial phase of operations (73 MW), while #2 and #4, with a fusion power of 500 MW, require a total additional heating power of 100 MW. The scenarios #1, #2 and #3 use full-size plasmas (R/a = 6.2 m/2.0 m) and #4 uses the plasma with a smaller minor radius (R/a = 6.35 m/1.85 m). This plasma can be produced in the vacuum vessel of ITER by shifting the magnetic axis outward. In this case, the plasma elongation can be increased to 1.8. These scenarios are also consistent with the magnet system.

The advantage of scenarios using a plasma with smaller minor radius is a longer burn time, consequent to the smaller plasma current, larger required β_N and available bootstrap current fraction. These scenarios show that very long pulse operation regimes are accessible in ITER with a modest improvement.

If the erosion due to Type I ELMs gives a short life time of the divertor target, a hybrid operation with a larger q_{95}, typically ≥ 3.5, and small ELMs would be suitable for high fluence tests. One possible example is Hybrid #3 shown in Table 4.3.2-1.

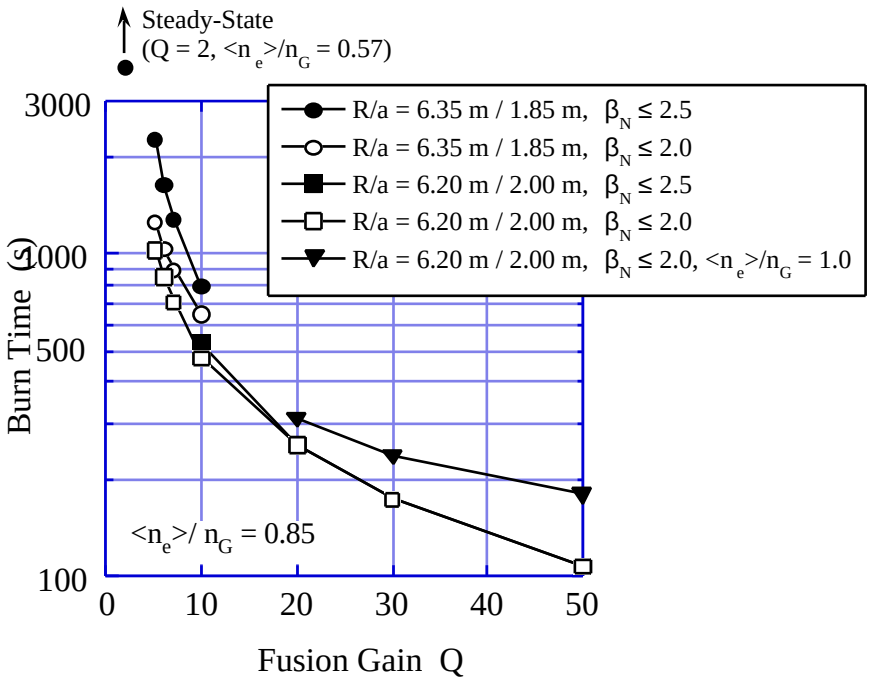

Figure 4.3.2-1 Fusion Gain and Burn Time for Hybrid Mode of Operation

The results for plasmas with smaller minor radius (R/a/κ = 6.35 m/1.85 m/1.8) are also shown. (This plasma can be produced in the ITER vacuum vessel by shifting the magnetic axis outward.)

Table 4.3.2-1 PRETOR Simulation Results for Hybrid Operations

	Scenario 3			
	Hybrid #1	Hybrid #2	Hybrid #3	Hybrid #4
R (m)/a (m)	6.2/2.0	←	←	6.35/1.85
κ_{95}/δ_{95}	1.7/0.33	←	←	1.8/0.35
V_P (m^3)	831	←	←	770
B_T (T)	5.3	←	←	5.17
I_P (MA)	13.8	14.4	13.3	12.6
q_{95}	3.3	3.2	3.5	3.1
$<n_e>$ ($10^{19}m^{-3}$)	9.3	10.0	9.0	11.0
$<n_e>/n_G$	0.85	←	←	0.94
$<T_i>$ (keV)	8.4	9.4	8.2	8.5
$<T_e>$ (keV)	9.6	10.9	9.1	9.7
β_N	1.9	2.2	1.9	2.3
P_{FUS} (MW)	400	500	350	500
P_{NB} (MW)	33	60	33	60
P_{RF} (MW)	40	40	40	40
$Q = P_{FUS}/(P_{NB}+P_{RF})$	5.4	5.0	4.8	5.0
P_{LOSS}/P_{L-H}	114/45	151/47	113/45	154/47
τ_E (s)	2.73	2.40	2.62	2.26
$f_{He,\,axis/ave}$ (%)	3.5/2.5	3.9/2.7	2.9/2.2	3.3/2.5
$f_{Ar,\,axis}$ (%)	0.19	0.25	0.15	0.20
$Z_{eff,\,ave}$	1.85	2.03	1.73	1.88
P_{RAD} (MW)	55	72	44	67
P_{Sep} (MW)	99	128	100	133
β_p	0.76	0.83	0.77	1.01
l_i (3)	0.91	0.87	0.88	0.81
I_{CD}/I_P (%)	25	32	28	29
I_{BS}/I_P (%)	17	20	18	21
γ_{20}^{NB} (10^{20}A/Wm^2)	0.24	0.26	0.26	0.23
γ_{20}^{RF} (10^{20}A/Wm^2)	0.30	←	←	←
γ_{20}^{TOT} (10^{20}A/Wm^2)	0.27	0.27	0.28	0.26
τ_{He}^*/τ_E	5	←	←	←
$H_{H98(y,2)}$	1.0	←	←	←
V_{loop} (mV)	56	46	53	46
Burn flux (Vs)	60	56	68	74
Burn time (s)*	1070	1220	1280	1610

* Burn time for the case that the flux used during the heating phase is saved

4.3.3 Steady State Operation Scenario

In the steady state (SS) operation scenario the total plasma current at the current flat-top phase is generated non-inductively by additional current drive (NB and RF) and bootstrap current. A conventional ELMy H-mode with $H_{H98(y,2)}$ gives a low Q, i.e., Q ~2 in a steady state operation. To provide SS operation in ITER with Q > 5 with the available additional power (P_{NB} < 50 MW,P_{IC} + P_{EC} + P_{LH} < 80 MW) it would be necessary to decrease the plasma current to I_p ~ 9 MA. In this case the bootstrap current fraction will increase due to an increase of the poloidal beta (I_{bs}/I_p β_p I_p^{-1}). To obtain the required CD efficiency for full steady state operation with Q > 5, an improved confinement with $H_{H98(y,2)}$ ~ 1.5-1.6 is necessary. In present-day experiments such confinement is achieved and sustained up to ~2.6 s in regimes with specially shaped safety factor profiles, associated with internal transport barriers (ITB)[1,2]. The ITB appears in the discharges with strong negative shear (SNS) with q(0) ~q_{95} ≥ q_{min} ≥2, weak negative shear (WNS) with q_{95}> q(0) > q_{min} > 1, or weak positive shear rq′/q < 1 (WPS) with q(0) > 1.

An example set of steady-state plasma parameters and profiles for WNS snenario is shown in Table 4.3.3-1 and Figure 4.3.3-1. Here, the 1st NB is injected at the position closest to the magnetic axis (distance from the magnetic axis ΔZ ~ 0.38 m at R = 6.2 m) and the 2nd NB is injected at the outer most position (ΔZ ~ 0.95 m). LH power is also injected at R_{LH}-R=1.25m and the normalized current drive efficiency is assumed to $\gamma_{20} = 0.3 A w^{-1} m^{-2}$. In this scenario, the zone of the improved confinement propagates to 70% of the minor radius but the central electron and ion temperatures are moderate because of high neoclassical heat conductivity χ_{iNeo}. The shape of the profiles is similar to what is obtained in some present day ITB experiments1.

[1] F.X. Soldner et al , Nucl. Fus. **39** (1999) 407
[2] Y. Kamada and the JT-60 Team, “Extended JT-60U Plasma Regimes toward High Integrated Performance”, in Proc. 18th IAEA Fusion Energy Conference, Sorrento, Italy, (2000), IAEA-CN-77/OV1/1

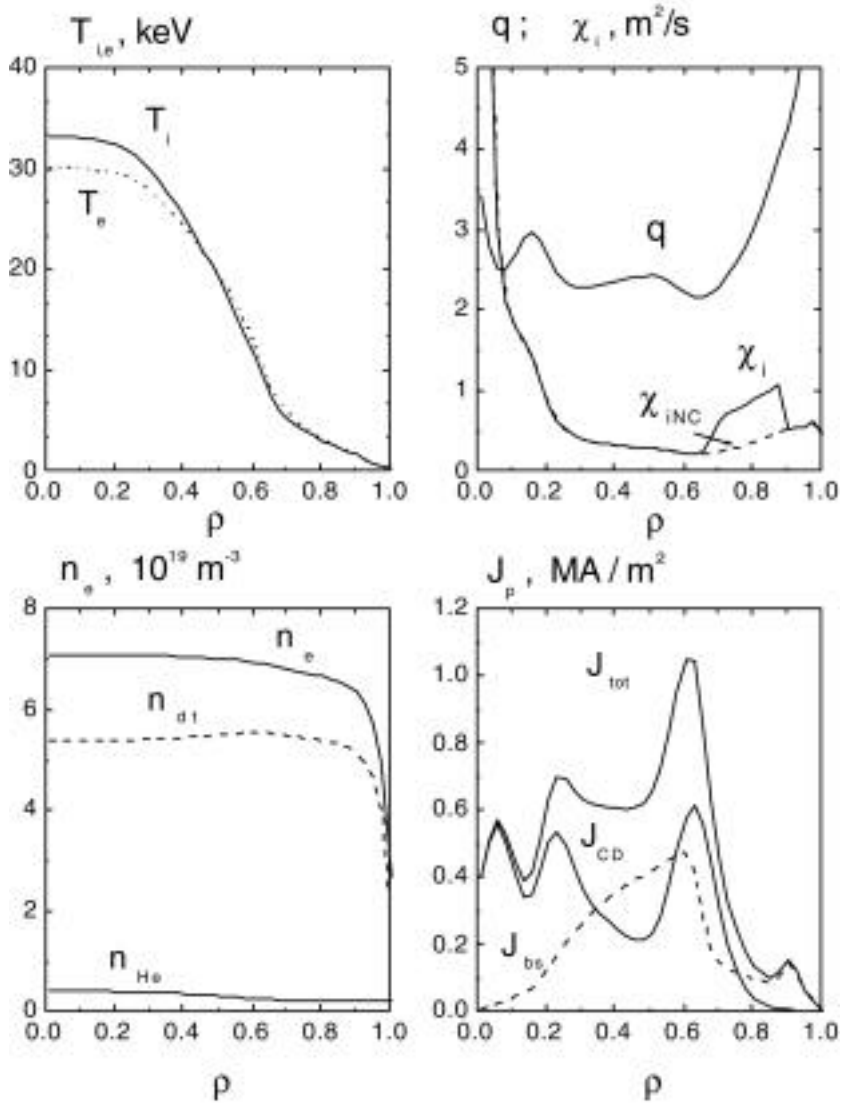

Figure 4.3.3-1 Plasma Parameter Profiles at the Current Flat-top phase (t > 1000 s) for the Steady-state WNS Operational Scenario

Table 4.3.3-1 ITER Parameters for the Non-Inductive Scenario

Parameter	WNS	Parameter	WNS	Parameter	WNS
R/a (m/m)	6.35/1.85	β_N	2.95	f_{He} (%)	4.1
B_T (T)	5.18	β_p	1.49	f_{Be} (%)	2
I_p (MA)	9.0	P_{fus} (MW)	356	f_{Ar} (%)	0.26
κ_{95}/δ_{95}	1.85/0.4	$P_{L-H} + P_{NB}$ (MW)	29 + 30	Z_{eff}	2.07
$<n_e>$ ($10^{19}m^{-3}$)	6.7	Q	6.0	P_{rad} (MW)	37.6
n/n_G	0.82	W_{th} (MJ)	287	P_{loss} (MW)	92.5
$<T_i>$ (keV)	12.5	$P_{loss}/P_{thr. L-H}$	2.59	τ_E (s)	3.1
$<T_e>$ (KeV)	12.3	β_T %	2.77	τ_α^*/τ_E	5.0
I_{CD}/I_p (%)	51.9	l_i (3)	0.72	$H_{H98\,(y2)}$	1.57
I_{bs}/I_p (%)	48.1	$q_{95}/q_o/q_{min}$	5.3/3.5/2.2		
I_{OH}/I_p (%)	0				

4.4 Plasma Performance Assessment

4.4.1 Flexibility and Plasma Performance Optimisation

4.4.1.1 Operation Boundary

The operation domain plot in H_H factor and fusion power space is a useful tool to analyse the performance of ITER. Figure 4.4.1-1 shows such a plot resulting from 1.5D simulations using PRETOR[1]. Here, the fusion power as a function of $H_{H98(y,2)}$ for various operation conditions is presented when I_P = 15 MA. Each point of the domain corresponds to a fusion gain Q = 10. Here, β_N is the normalised beta, n_G is the Greenwald density P_{LOSS} is the power across the H-mode edge pedestal and P_{L-H} is the power required for the H-mode transition[2]. The power assumed to be required for a good confinement is $1.3\times P_{L-H}$. When $H_{H98(y,2)}$ = 1.0 and $<n_e>/n_G$ = 0.85, 400 MW of fusion power is produced.

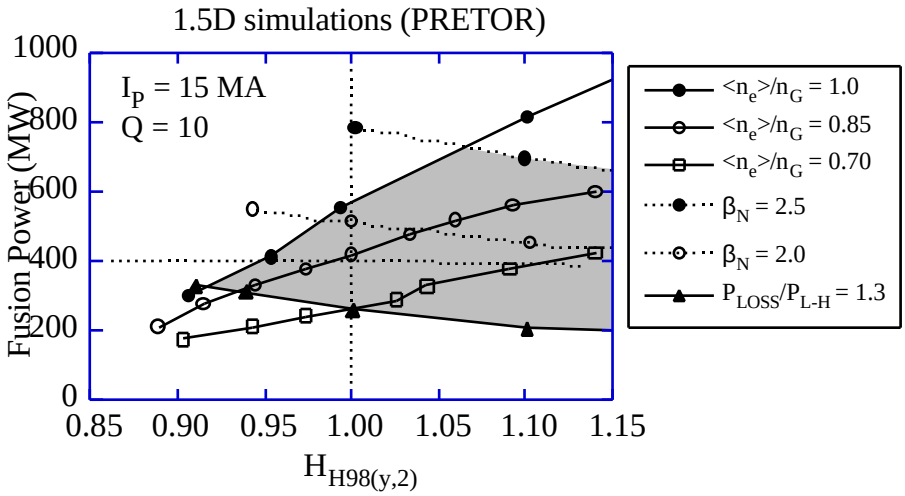

Figure 4.4.1-1 Operation Domain in H_H-factor and Fusion Power Space when I_P = 15 MA and Q = 10

If the operation boundaries are given by $<n_e>/n_G$ = 1.0, β_N = 2.5 and P_{LOSS}/P_{L-H} = 1.3 (shaded area in the figure), the maximum and minimum fusion powers are 560 MW (point B) and 260 MW, respectively, when $H_{H98(y,2)}$ = 1.0. It is also seen that about 8 % of confinement margin (margin in H_H factor to achieve operation with Q = 10) exists.

A possible range of Q is given in Figure 4.4.1-2, showing results of PRETOR calculations of fusion power, Q values, $<T_e>$, $<T_i>$, β_N, f_{Ar}, Z_{eff}, P_{BRM}, P_{LIN}, and P_{SYN} as a function of P_{ADD} for a plasma with I_P = 15 MA, $\tau_{He}^*/\tau_E \sim 5$ and $<n_e> = 1.19\times10^{20}m^{-3}$ ($<n_e>/n_G$ = 1.0). Ar is seeded to limit $P_{Divertor} \sim 30$ MW($\sim$5 MWm^{-2}). As the additional heating power is reduced, Q increases, to exceed 20 at Padd $\leq$ 20 MW. The upper limit of Q is determined by the H-L transition. The boundary given by the condition of P_{LOSS} greater than than 1.3 x P_{L-H} is indicated in the Figure.

[1] D. Boucher, et al., in Proc. 16th IAEA Fusion Energy Conference, Montreal, 1996 (IAEA,Vienna, 1997) 945
[2] ITER Physics Basis, Nucl. Fus. **39** (1999) 2137

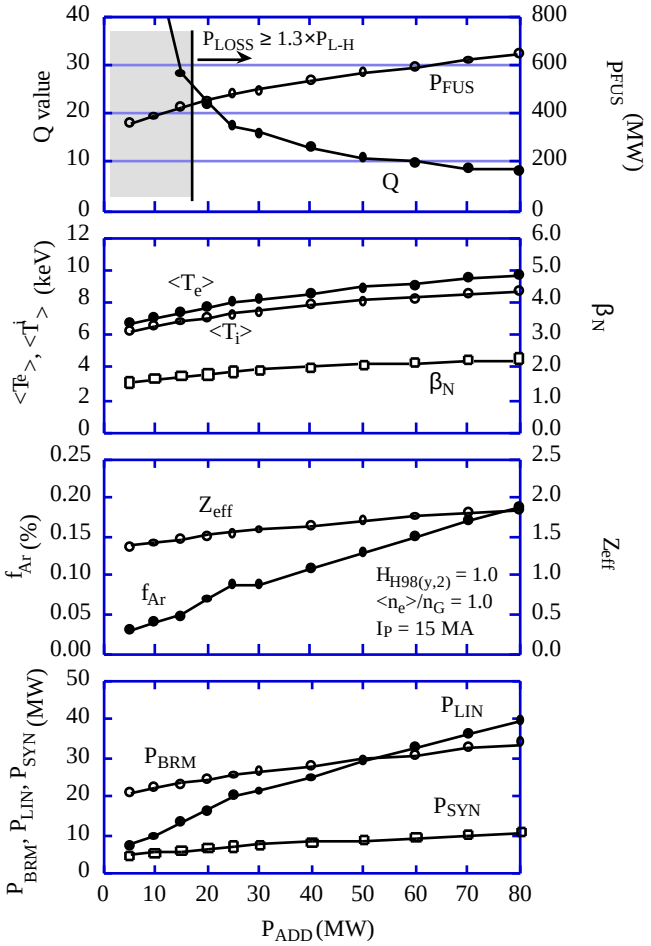

Figure 4.4.1-2 1.5D Simulation Results of Plasma Performance
Here, $I_P = 15$ MA, $\tau_{He}^*/\tau_E = 5$ and $<n_e> = 1.19\times10^{20}m^{-3}$ ($<n_e>/n_G = 1.0$).
Ar is seeded to limit $P_{Divertor} \sim 30$ MW(~ 5 MW/m^2)

4.4.1.2 Sensitivity Analyses

(1) Density and temperature profile effects

In general, peaked density profiles tend to produce larger fusion power for the same average density and even more for the same pedestal density. Here, the density profile effect is examined by including the inward pinch effect, as an example. This kind of profile could be achieved also with deep fuelling by high field side (HFS) pellet injection. Figure 4.4.1-3-a shows the density profiles when a pinch term proportional to the thermal diffusivity χ and to the magnetic shear is included with a different pinch coefficient V_P. In this modelling, the pinch effect is not significant in the core region ($r/a < 0.5$) where the shear is small. Figure 4.4.1-3-b shows the fusion power for various pinch coefficients. Here, the volume-averaged density is fixed to $1.0\times10^{20}m^{-3}$, which corresponds to $n_e/n_G = 0.85$ for the flat profile. It is seen that significantly higher fusion power is available in the nominal to high H_H factor region, while the margin below 1.0 in H_H factor is not increased in the lower fusion power region. Helium accumulation due to the pinch effect also degrades performance. If a peaked density profile is achieved by using HFS pellet injection, a more significant improvement is expected.

(2) Dependence on χ_i/χ_e ratio

The ratio of ion thermal diffusivity to electron thermal diffusivity χ_i/χ_e is assumed to be 2 for the reference case with additional dependencies such as $(T_e/T_i)^{0.5}$. This χ_i/χ_e value was chosen as a conservative assumption although $\chi_i/\chi_e < 1$ is obtained in many experiments. Figure 4.4.1-4 shows the relation between χ_i/χ_e and fusion power for two types of transport coefficients profiles, the RLWB model[1] and parabolic model ($\chi_e = c_0(1+4(r/a)^2)$) both with normalisation factor c_0. It is seen that the fusion power increases with decreasing χ_i/χ_e for both models and the present assumption ($\chi_i/\chi_e = 2$) is conservative.

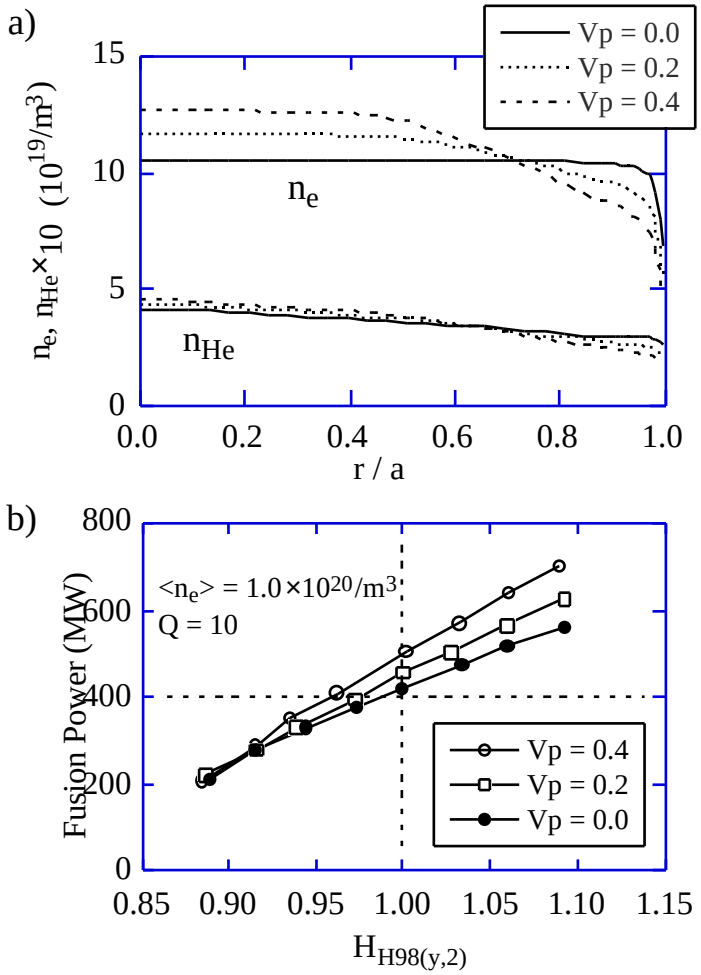

Figure 4.4.1-3 a) Density Profiles for Various Pinch Coefficients V_p, b) Dependence of Fusion Power on the H_H Factor for the Pinch Coefficients shown in (a)

[1] D. Boucher and P-H. Rebut, in Proc. IAEA TCM on Advances in Simulations of Modeling of Thermonuclear Plasmas, 1992, IAEA, Vienna, (1993) 142

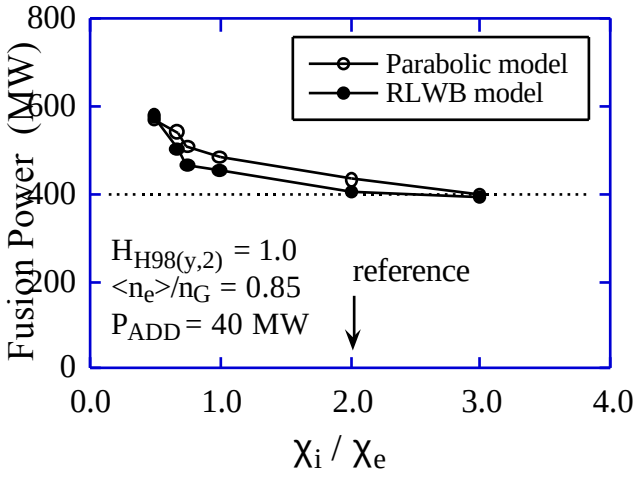

Figure 4.4.1-4 Dependence of Fusion Power on χ_i/χ_e when $H_{H98(y,2)}$ = 1.0, P_{ADD} = 40 MW and $<n_e>/n_G$ = 0.85

(3) Effect of ion heating fraction

The increase of the ion heating fraction is also favourable for the improvement of operation performance. Figure 4.4.1-5 shows the relation between the H_H factor and fusion power for different ion heating fractions P_i/P_{RF}. Here, all heating power is RF and the total heating power $P_{RF} = P_i+P_e$ is adjusted to Q = 10 with $<n_e>/n_G$ = 0.85. In the figure, the NB-heating-only case is also shown. It is seen that the fusion power increases with P_i/P_{RF} through the H_H range, and the lower H_H margin is also improved.

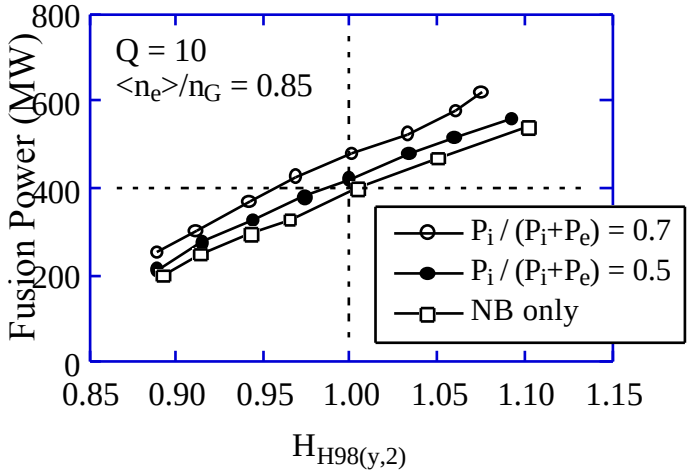

Figure 4.4.1-5 Dependence of Fusion Power on H_H-factor for Various Ion Heating Fractions

4.4.1.3 Operation with Higher Plasma Current, High Q and Ignited

One of the possible scenarios in ITER foresees a total plasma current up to 17MA albeit with some additional engineering margins which may or may not actually apply given inevitable conservatism in the design. Under the condition of an increased plasma current to 17 MA, clearly the operation boundary is significantly expanded, leaving ignition as a possibility even when $H_{H98(y,2)}$ = 1.0 and $<n_e>/n_G$ = 0.85.

Figure 4.4.1-6 shows the operation domain in $H_{H98(y,2)}$ and fusion power space when Q = 50 and I_P = 17 MA. If the operation boundaries are given by $<n_e>/n_G$ = 1.0 and P_{LOSS}/P_{L-H} = 1.3 (shaded area in the plot), the minimum and maximum fusion powers are 450 MW and 650 MW respectively, when $H_{H98(y,2)}$ = 1.0. It is also seen that operation with Q = 50 is possible with certain margin even if the density boundary is set to $<n_e>/n_G$ = 0.85.

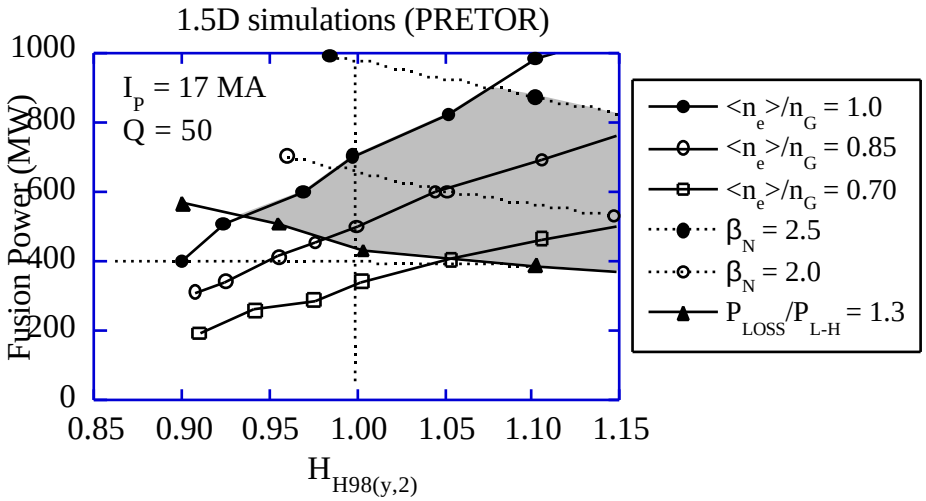

Figure 4.4.1-6 Operation Domain in H_H factor and Fusion Power Space when I_P = 17 MA and Q = 50

Figure 4.4.1-7-a shows PRETOR simulation results for high-Q operation when the plasma current is 17 MA and the electron density is $1.1\times10^{20}m^{-3}$ (~ $0.81\times n_G$). The helium accumulation is again calculated by assuming τ_{He}^*/τ_E = 5. During the plasma flat top, the additional heating power (P_{ADD}) is 10 MW and about 450 MW (Q = 45) of fusion power (P_{FUS}) is produced. In this scenario, 73 MW of additional heating power is required from 10 s to 13.5 s to achieve the H-mode transition. Here, P_{L-H} is the threshold power for the L-H transition and P_{LOSS} is the power across the H-mode pedestal. In the early phase of the discharge, fusion power excursion is observed. This result implies that ignition is possible by turning off the additional heating power for a short period.

Figure 4.4.1-7-b shows a simulation for a fully ignited operation. The heating power P_{ADD} is turned off at t = 13.5 s and other assumptions are the same as for Figure 4.4.1-7-a. When the heating power is turned off, the helium level is very small and the self-heating power is large enough for H-mode operation. Therefore, the ignition state is maintained for about 40 s and the L-mode transition occurs at t = 55 s. In this study, a hysteresis for HL-transition is conservatively not assumed.

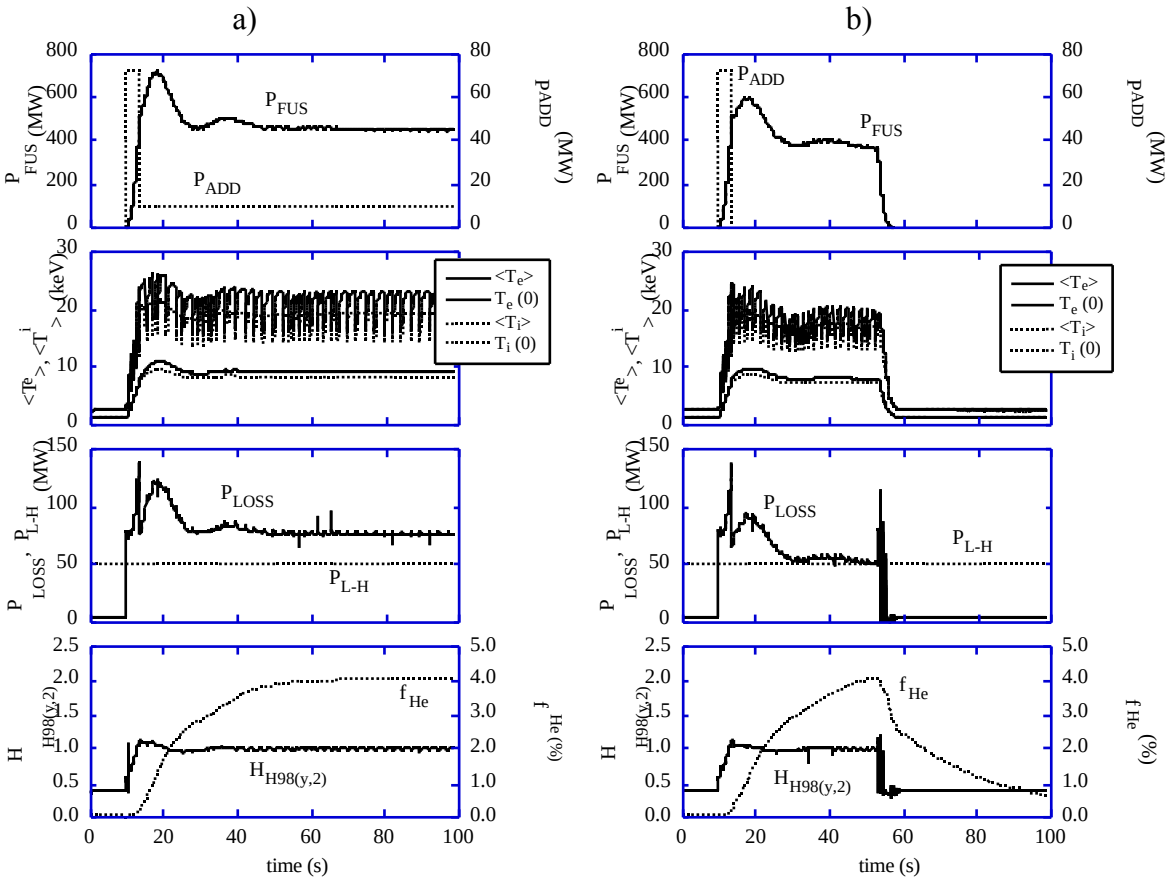

Figure 4.4.1-7 Time Evolution of Plasma Parameters for High-Q Operation
I_P = 17 MA, $\langle n_e \rangle = 1.1\times10^{20}/m^3$ ($\langle n_e \rangle / n_G = 0.81$) and $\tau_{He}^*/\tau_E = 5$. a) Q = 45, b) Q = ∞

Since the pumping rate can be increased up to 400 Pa m^3s^{-1} for a short period, operation with $\tau_{He}^*/\tau_E < 5$ could be even more likely. Figure 4.4.1-8 shows the results for various helium accumulation levels. The ignition operation continues in steady state when $\tau_{He}^*/\tau_E = 4$. It is seen that the transient ignition experiment can be performed even for lower pumping efficiency ($\tau_{He}^*/\tau_E = 7$).

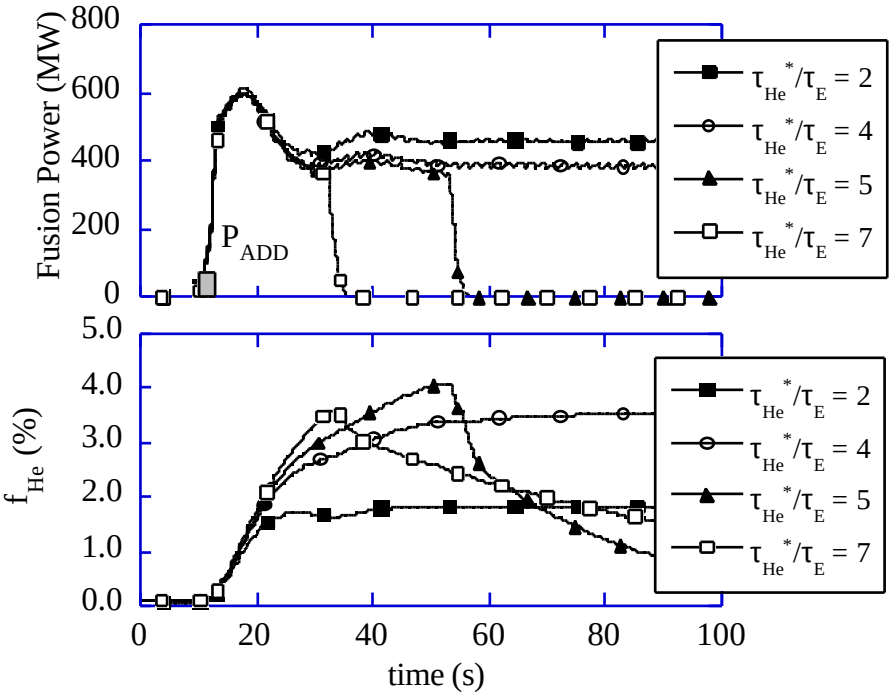

Figure 4.4.1-8 Time Traces of Fusion Power and Helium Fraction for Various τ_{He}^* Assumptions

Here, I_P = 17 MA, $\langle n_e \rangle = 1.1 \times 10^{20} m^{-3}$ ($\langle n_e \rangle / n_G = 0.81$) and P_{ADD} = 73 MW from t = 10 s to t = 13.5 s. L-mode transition occurs when $P_{LOSS} < P_{L-H}$.

4.4.2 Projection of Steady-State Operation and Assessment

Here, the SS operation scenario is described on a basis similar to present day experiments. The results of 1.5D transport simulations with ASTRA code[1] are presented. In these analyses, realistic NBH&CD modelling[2] in ITER geometry has been used. ECCD parameterisation for absorption width and CD efficiency has been computed based on the OGRAY simulations[3], and for LHCD a semi-empirical approach was utilized, prescribing absorption width and position (in the outer region r/a > 0.5) with a CD efficiency γ_{20} = 0.3 $AW^{-1}m^{-2}$. The plasma parameters for WNS, WPS, SNS and Low-Q scenarios are presented in Table 4.4.2-1. Absence of q = 2, 1.5 and 1 surface inside the plasma eliminates the growth of tearing modes.

[1] G.V. Pereverzev, et al., IPP 5/42 (1991)
[2] A.R. Polevoi, T. Takizuka, H. Shirai, "Benchmarking of the NBI Block in ASTRA Code Versur the OFMC Calculations, JAERI Data/Code 97-014, (1997)
[3] A.V. Zvonkov, A.Yu. Kuyanov, A.A. Skovoroda, and A.V. Timofeev, Plasma Phys. Rep., **24** (1998) 389

Table 4.4.2-1 Parameters for Non-Inductive Scenarios at the Flat Top

		Scenario 4		Scenario 6	Scenario 7
		WNS	WNS	SNS	WPS
R/a	(m)	6.35/1.85	6.35/1.85	6.35/1.85	6.35/1.85
B_T	(T)	5.18	5.18	5.18	5.18
I_P	(MA)	9.0	9.5	9.0	9.0
κ_{95}/δ_{95}		1.85/0.40	1.87/0.44	1.86/0.41	1.86/0.41
$<n_e>$	($10^{19}m^{-3}$)	6.7	7.05	6.5	6.7
n/n_G		0.82	0.81	0.78	0.82
$<T_i>$	(keV)	12.5	11.6	12.1	12.5
$<T_e>$	(keV)	12.3	12.6	13.3	12.1
β_T	(%)	2.77	2.67	2.76	2.75
β_N		2.95	2.69	2.93	2.92
β_p		1.49	1.25	1.48	1.47
P_{fus}	(MW)	356	338	340	352
$P_{LH} + P_{NB}$	(MW)	29 + 30 *1	28 + 35	40 + 20 *2	29 + 28 *3
$Q = P_{fus}/P_{add}$		6.0	5.36	5.7	6.2
W_{th}	(MJ)	287	272	287	285
P_{loss}/P_{LH}		2.59	2.74	2.63	2.6
τ_E	(s)	3.1	2.92	3.13	3.07
f_{He}	(%)	4.1	4.0	4.0	4.0
f_{Be}	(%)	2	2	2	2
f_{Ar}	(%)	0.26	0.16	0.2	0.23
Z_{eff}		2.07	1.87	1.89	1.99
P_{rad}	(MW)	37.6	30.6	36.2	34.6
P_{loss}	(MW)	92.5	93.2	91.6	92.7
l_i (3)		0.72	0.43	0.6	0.69
I_{CD}/I_p	(%)	51.9	49.7	53.7	50.2
I_{bs}/I_p	(%)	48.1	50.3	46.3	49.8
I_{OH}/I_p	(%)	0	0	0	0
$q_{95}/q_o/q_{min}$		5.3/3.5/2.2	5.01/3.8/2.7	5.4/5.9/2.3	5.3/2.7/2.1
$H_{H98(y2)}$		1.57	1.46	1.61	1.56
τ_{He}^*/τ_E		5.0	5.0	5.0	5.0

1 ΔZ1(NB) ~0.38 m (P = 0.5 P_{NB}), ΔZ2(NB) ~0.95 m (P = 0.5 P_{NB}), R_{LH} - R = 1.28 m (γ = 0.3A/Wm^2)
2 ΔZ1(NB) ~0.38 m (P = 0.35 P_{NB}), ΔZ2(NB) ~0.95 m (P = 0.65 P_{NB}), R_{LH} - R = 1.2 m (γ = 0.3A/Wm^2)
3 ΔZ1(NB) ~0.38 m (P = 0.67 P_{NB}), ΔZ2(NB) ~0.95 m (P = 0.33 P_{NB}), R_{LH} - R = 1.37 m (γ = 0.3A/Wm^2)

4.4.2.1 Weak Negative Shear Scenario

After the plasma initialisation phase, the plasma current profile is almost flat with high central q(0) ~ 2. Such a profile is close to the desirable one during the current flat-top phase.

To prevent current peaking, a fast current ramp-up rate and an additional heating power are required.

After the X-point formation, the RF heating power is increased gradually to 29 MW to provide the L-H transition at low density. Each of two NB injectors (on-axis and off-axis) delivers 15 MW. The gradual replacement of carbon by argon keepsthe loss power from the core to the separatrix at a level compatible with the divertor constraints, i.e. $P_{loss} < 100$ MW.

In the considered scenario the resistive voltage drops to zero in ~ 100 s. A complete steady-state current profile relaxation takes about 2000 s. The steady-state plasma profiles of scenario 4 are presented in Figure 4.2.3-1. The scenario 4 requires $\beta_N = 2.95$, which is slightly above the no-wall limit (~ 4 $l_i = 2.88$). The second scenario of WNS requires a lower value of $\beta_N = 2.69$, but li is low (4 $l_i = 1.72$).

4.4.2.2 Strong Negative Shear Scenario

Early application of 9 MW of ECRH power and 2 MW of RFheating power increases the skin time and prevents the current redistribution. After the X-point formation the RFpower is increased to 40 MW to provide the L-H transition. After the density reaches sufficiently high value, neutral beam injection is started and P_{NB} increases to 20 MW.

The high central q values would increase alpha particles losses and reduce plasma performance. For these reasons the SNS configuration looks less promising for ITER SS operation. In all of these regimes, Q > 5, but the normalised beta exceeds the ideal mhd limit without wall, thus requiring stabilization of resistive wall modes (RWMs).

4.4.2.3 Weak Positive Shear Scenario

The waveforms of plasma parameters in the WPS scenario are similar to those in the WNS scenario. The main difference is in the redistribution of the NB power 2/3 of which should be injected near the plasma centre. In the WPS scenario the target central q value is smaller, so 5 MW of the ECRH power is applied later.

4.5 Divertor and Edge Pedestal

4.5.1 Divertor Performance

Divertor modelling with the B2-Eirene code package[1,2] has become an important tool in the ITER divertor design. This code, which is constantly validated against data from various experiments, predicts the divertor plasma performance in ITER and its dependence on geometry[3] as well as on various other parameters[1] (e.g. gas throughput, upstream density n_s,

[1] D. Reiter, H. Kever, G.H. Wolf, et al., Plasma Phys. and Contr. Fusion, **33** (1991) 1579
[2] R. Schneider, D. Reiter, H-P. Zehrfeld, et al. J. Nucl. Mater., **196–198** (1992) 810
[3] A.S. Kukushkin, G. Janeschitz, A. Loarte, et al., "Critical Issues in Divertor Optimisation for ITER-FEAT", Proc. 14th PSI Conference, Rosenheim, 2000 (to be published in J. Nucl. Mater.)

etc.). The fact that similar behaviour can be found in experiments on JET and other divertor tokamaks gives credibility to these modelling results and allows their use as design guidance.

Most of the modelling studies performed to date assume CFC-clad vertical targets in the strike zone areas and W cladding on all other surfaces. While self-consistent sputtering and impurity transport of W is not treated in the code calculations, the self-consistent behaviour of C is taken into account by assuming physical sputtering as well as chemical sputtering, the latter with a constant yield of 1%. Thus the main radiation losses in the SOL and in the divertor originate from carbon radiation. A few calculation runs were performed assuming a pure W divertor and N, Ne or Ar seeding in order to replace the C radiation losses. In all cases a Z_{eff} at the core-edge interface (CEI, a surface assumed ~ 5 cm inside the separatrix at the outer equator) and at the separatrix is calculated taking He and other impurities such as C, N, Ne and Ar into account. Note that no realistic transport model for the region inside the separatrix, which would correctly describe the "transport barrier" and "pedestal" physics is implemented in the code. At the same time, the relation between the divertor performance and the upstream plasma parameters at the separatrix is insensitive to the detail of the transport inside the separatrix, therefore the interface parameters such as Z_{eff} or helium concentration are in most cases determined at the separatrix.

4.5.1.1 Target Geometry

It was found[3] that the peak power loads on the divertor targets depend strongly on the arrangement of the divertor target, and the bottom part of the divertor chamber. If the bottom part of the divertor chamber makes a distinct corner (V shape) with the target, and if the separatrix strike-point is located near this corner (Figure 4.5.1-1), then the neutrals become locked in the vicinity of the strike-point, thus favouring partial detachment at the separatrix. The results are consistent with experiments at JET for which the strike point was swept across the target[2]. The effect is strong: introduction of a V, about 10 cm deep near the separatrix strike-point, reduces the peak power load by 30% compared with a straight vertical target for ITER conditions. This can outweigh the effect of the variation of the divertor length or the divertor closure. Optimisation of the divertor geometry and pumping speed reduces the power loading further. A reduction of the pumping speed causes a similar effect, i.e. increased neutral pressure in the divertor and reduced power load, but leads to a deterioration of helium removal - which is not the case for the modification of the target shape.

[1] A.S. Kukushkin, et al., "Basic Divertor Operation in ITER-FEAT", 18th IAEA Fusion Conference, Sorrento, Italy, Oct. 2000
[2] A. Loarte, Nucl. Fus. **38** (1998) 587 R. Monk, et al., Proc. 24th EPS Conf. Contr. Fusion Plasma Phys., Berchtesgaden, 1997, Vol. 21A (1997) 117

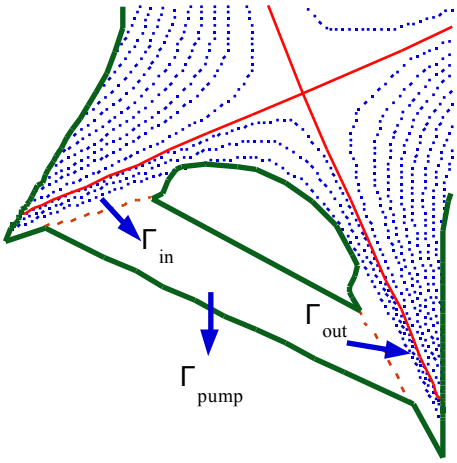

Figure 4.5.1-1 Divertor Geometry Used in the Calculations
Arrows indicate the direction of neutral flows in the private flux region. The dome-supporting structures are represented by two surfaces (dotted lines) with transparency of 0.56 for the neutrals

4.5.1.2 Gas Flow Between the Divertors

Gas conductance in the private flux region (PFR) between the inner and outer divertors also plays an important role. Indeed, because the neutral pressure in the inner divertor is normally higher than in the outer, the resultant gas flow between the divertors increases the neutral-induced energy loss in the outer divertor and thus reduces the power loading there. In a real divertor, there are supporting structures beneath the dome which hinder the gas flow. This effect was modelled[1] by introducing two semi-transparent surfaces connecting the dome edges with the divertor bottom, as in Figure 4.5.1-1. The effect is clear: reduction of the gas conductance between the divertors results on the whole in a considerable, up to a factor 2, increase of the peak power loading. This observation is consistent with JET experiments[2], where the introduction of a "septum" separating the inner and outer divertors was found to increase the asymmetry of the divertor parameters, i.e., the outer divertor became hotter and the inner one more detached. In that experiment, it was found that symmetry of the divertor parameters can be recovered by gas puffing in the outer divertor and pumping from the inner. However, this approach is not feasible in ITER because the gas throughput between the divertors at fully transparent structures in PFR is calculated to be 300 to 400 Pam^3/s which is far beyond the pumping capability of ITER (200 Pam^3/s). Sufficient gas conductance between the divertors in the PFR is therefore necessary in ITER.

4.5.1.3 Operational Window

The window for divertor operation in ITER is delimited by several constraints arising from core plasma and technology requirements.

[1] A.S. Kukushkin, et al., "Basic Divertor Operation in ITER-FEAT", 18th IAEA Fusion Conference, Sorrento, Italy, Oct. 2000
[2] C.F. Maggi, et al., Proc. 26th EPS Conf. on Contr. Fusion and Plasma Phys., Maastricht, 1999, ECA Vol. 23J (1999) 201

First, the divertor plasma must be compatible with core plasma conditions ensuring the necessary reactor performance, as given by core plasma modelling for ITER. The upstream plasma density at the separatrix, n_s, which is the edge density for the core plasma, is expected to be limited from one-third to two thirds of the core density. In a reference inductive operation, an edge density equal to $3.3\times10^{19}m^{-3}$ is therefore taken as a conservative assumption. The helium concentration in the core, $c_{He,}$ is limited by fuel dilution. Z_{eff} at the core is limited by the acceptable impurity radiation and fuel dilution. The values of c_{He} and Z_{eff} at the separatrix are taken as representative for the core plasma. The particle control in the recent calculations is accomplished by specifying the gas puffing rate (puffing from the top of the plasma), the pumping speed (the pumping duct is located in the PFR, beneath the dome), and the plasma flow from the core. The difference between the latter and the calculated neutral flow into the core is supposed to be balanced by some deep core fuelling $\Gamma_{core} \geq 0$ provided by e.g. pellet injection. The value of the neutral flux Γ_0 crossing the separatrix and providing the ion source in the core plasma should be compatible with the core conditions – that is, sufficient to maintain the density pedestal and low enough not to cause deterioration of the core confinement. In fact, in all calculations performed to date, less than 20% of the gas fuelled into the main chamber cross the separatrix as neutrals – i.e., the neutral influx into the core does not exceed about 50 Pam^3/s.

Secondly, the plasma parameters must be compatible with various technological requirements. The peak power on the targets, q_{pk}, must be below a certain value to satisfy constraints on the plasma-facing components (20 MW/m2 is the maximum limit and 10 MW/m^2 or less is desirable.). The particle throughput, Γ_{DT}, is limited by the capacity of the pumping and tritium processing facility and tritium inventory considerations. Γ_{core} is limited above by the capacity of the core fuelling system (pellet injection, neutral beams). Other constraints could arise from wall and target erosion but these are not considered yet.

The limits of this operational window are given in Table 4.5.1-1. Different means to control the divertor operation can be used to explore the window. In recent calculations, the gas puffing rate was varied in order to achieve the desirable density variation. The core fuelling varied slightly (10 to 15 Pam^3s^{-1}) along with the change in the neutral influx across the separatrix. The pumping speed, S_p, was kept constant in the density scans and varied between scans. Impurity seeding (neon, nitrogen, or argon) was used to explore the margins in Z_{eff}. The input power, P_{in}, depends on the plasma core conditions and it has been varied from 86 MW (P_{fusion} = 410 MW, Q = 10, 30% core radiation) to 100 MW (P_{fusion} = 600 MW, Q = 24, 30% core radiation, or Q = 13, 40% core radiation) and to 130 MW (P_{fusion} = 600 MW, Q = 9, 30% core radiation). He production rate was consistent with the fusion power. The divertor geometry was also varied to optimise the divertor operation window.

Table 4.5.1-1 Limits of the Operational Window of the ITER Divertor for the Reference Inductive Operation

Peak power load on the targets	$q_{pk} \leq 10$ MW/m^2
D-T particle throughput	$\Gamma_{DT} \leq 200$ Pa·m^3/s (1.1 10^{23} s^{-1})
Core fuelling	$0 \leq \Gamma_{core} \leq 50$ Pa·m^3/s (2.7 10^{22} s^{-1})
Upstream plasma density	$n_s \sim 0.33\times10^{20}$ m^{-3}
Helium concentration in the core plasma	$c_{He} \leq 0.06$
Z_{eff} in the core plasma	$Z_{eff} \leq 1.6$
Neutral influx to the core	$\Gamma_0 \sim 50$ Pa·m^3/s (2.7 10^{22} s^{-1})

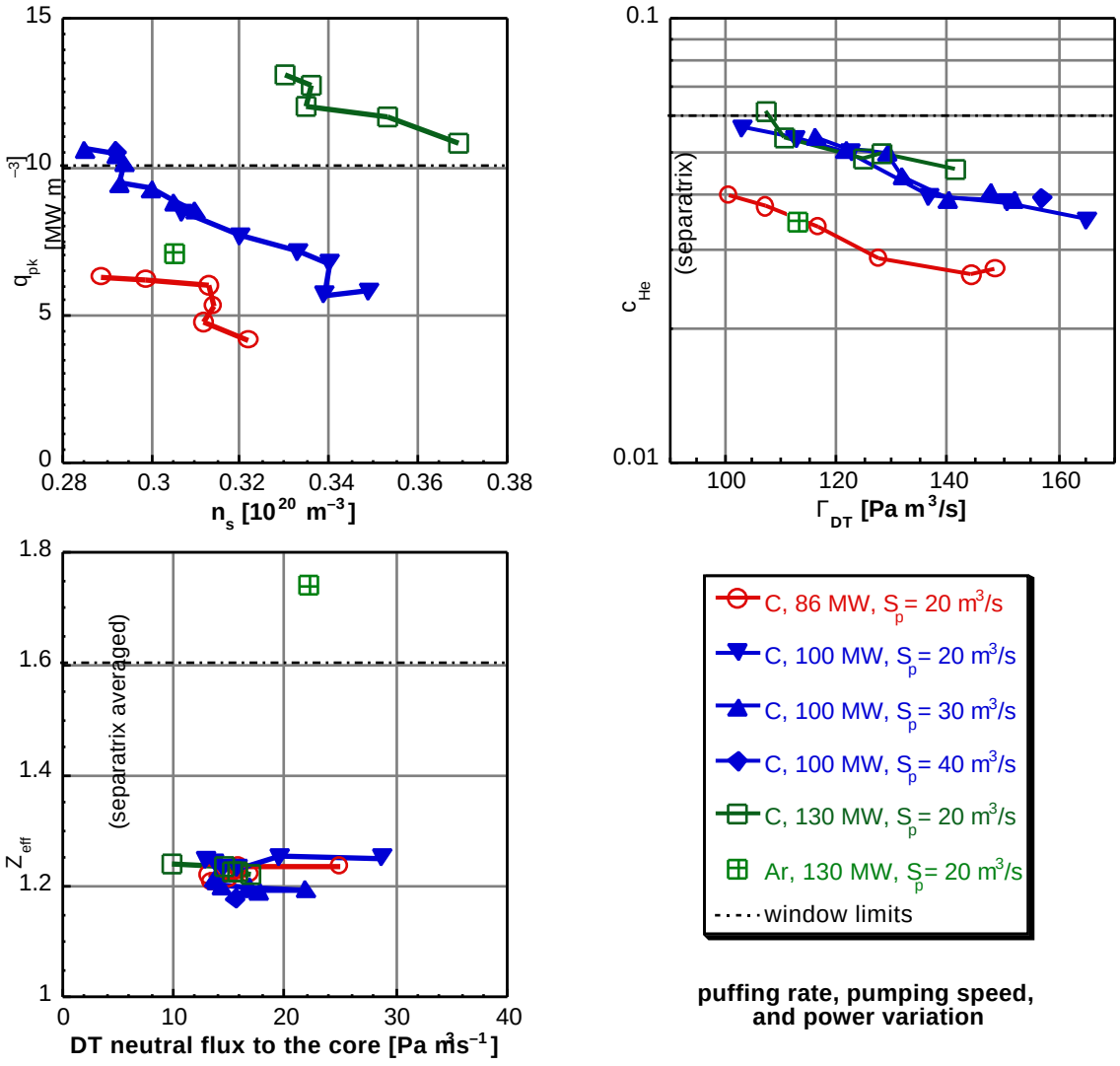

Figure 4.5.1-2 Three Views of the 6D Operational Window for the ITER Divertor, for V-shaped Carbon Targets, Varied Pumping Speed S_p, No Impurity Seeding, Three Levels of Input Power

A point for a full-tungsten target with argon-seeded plasma is also shown. The drops in peak power load at certain upstream densities are related to partial detachment at the inner and outer strike zone, respectively.

The 6-D operating window (q_{pk}, n_s, Z_{eff}, Γ_0, c_{He}, Γ_{DT}) for the reference ITER target geometry, Figure 4.5.1-1, is shown in Figure 4.5.1-2. Operational points inside the 6D window are seen to exist for the input power as high as 100 MW. Even at higher power, 130 MW, all the parameters except the peak power and upstream density are within the acceptable limits. If the restrictions on n_s can be relaxed (2/3 instead of 1/3 of the core density), then operation with higher input power becomes possible. There is a considerable margin in Z_{eff} for the carbon cases which implies a possibility of impurity seeding, and some margin in c_{He} which may be necessary to cope with the uncertainty of the helium transport in the core.

4.5.1.4 Pumping Speed

To trade off the margin in c_{He} against throughput, one can reduce the pumping speed to reduce the throughput while keeping the same neutral density in the divertor. Reducing the pumping speed leads to higher c_{He} at the same upstream density while the particle throughput goes down. It is therefore a control tool allowing, together with the fuelling rate, the plasma density and helium concentration to be tuned separately.

4.5.1.5 Impurity Seeding

Impurity seeding in addition to the sputtered carbon is not very efficient in enhancing the divertor radiation[1]. Indeed, radiation from seeded impurity reduces the power left for recycling, thus the particle flux to the surfaces drops together with the influx of sputtered carbon, resulting in a reduction of the radiation from carbon.

Another option would be to replace carbon completely with a seeded impurity. This could become necessary if carbon presence in the machine is deemed undesirable due to the tritium co-deposition problem. Limited modelling studies of the effect of this replacement were done for a simpler, straight target geometry. The results shown in Figure 4.5.1-3 suggest that the main trade-off is between the radiation power and Z_{eff} while the kind of seeded impurity is less important.

[1] A.S. Kukushkin, G. Janeschitz, A. Loarte, et al., "Critical Issues in Divertor Optimisation for ITER-FEAT", Proc. 14th PSI Conference, Rosenheim, 2000 (to be published in J. Nucl. Mater.)

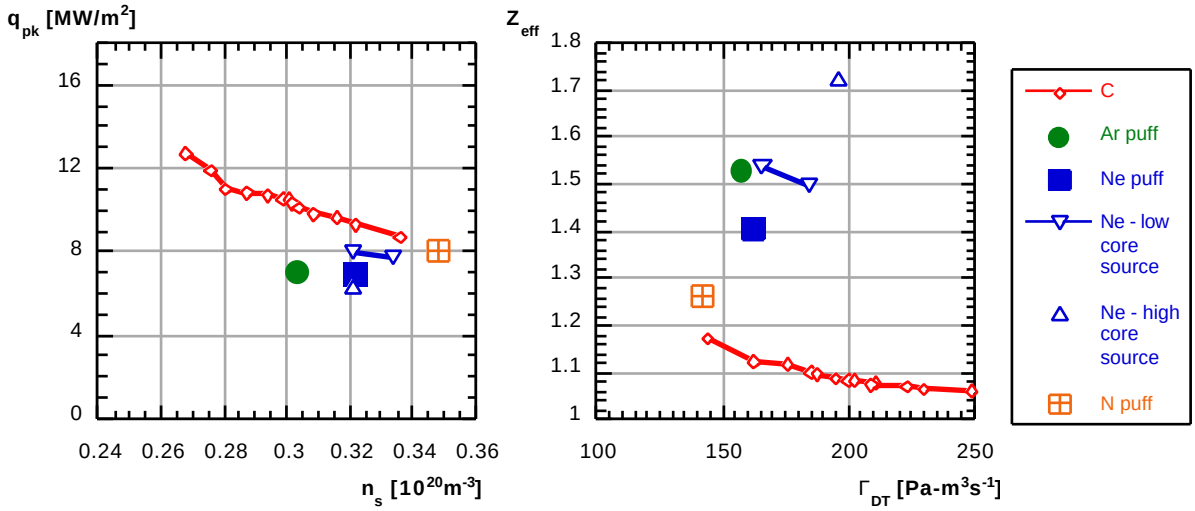

Figure 4.5.1-3 Divertor Performance with Impurity Seeding: Peak Power Loading vs. Upstream Plasma Density (left) and Z_{eff} at the Core-edge Interface vs. DT Particle Throughput (right)

The curve corresponding to the intrinsic carbon impurity as the radiator is also shown for comparison. The input power is 86 MW, pumping speed 75 m^3/s, straight target. The seeded impurity is either puffed as neutrals into the outer divertor (N, Ne, Ar) or supplied from the core as ions (Ne).

4.5.1.6 Prospects for Steady State Operation

Steady state operation with non-inductive current drive implies higher input power (low Q), lower upstream density, and greater connection length (high q). Initial studies done for the reference ITER geometry with reduced current and 100 MW input power show that the increase of the connection length reduces the q_{pk} at given n_s and improves helium pumping. At present, the results are only available for carbon divertor plates, without impurity seeding, Figure 4.5.1-4.

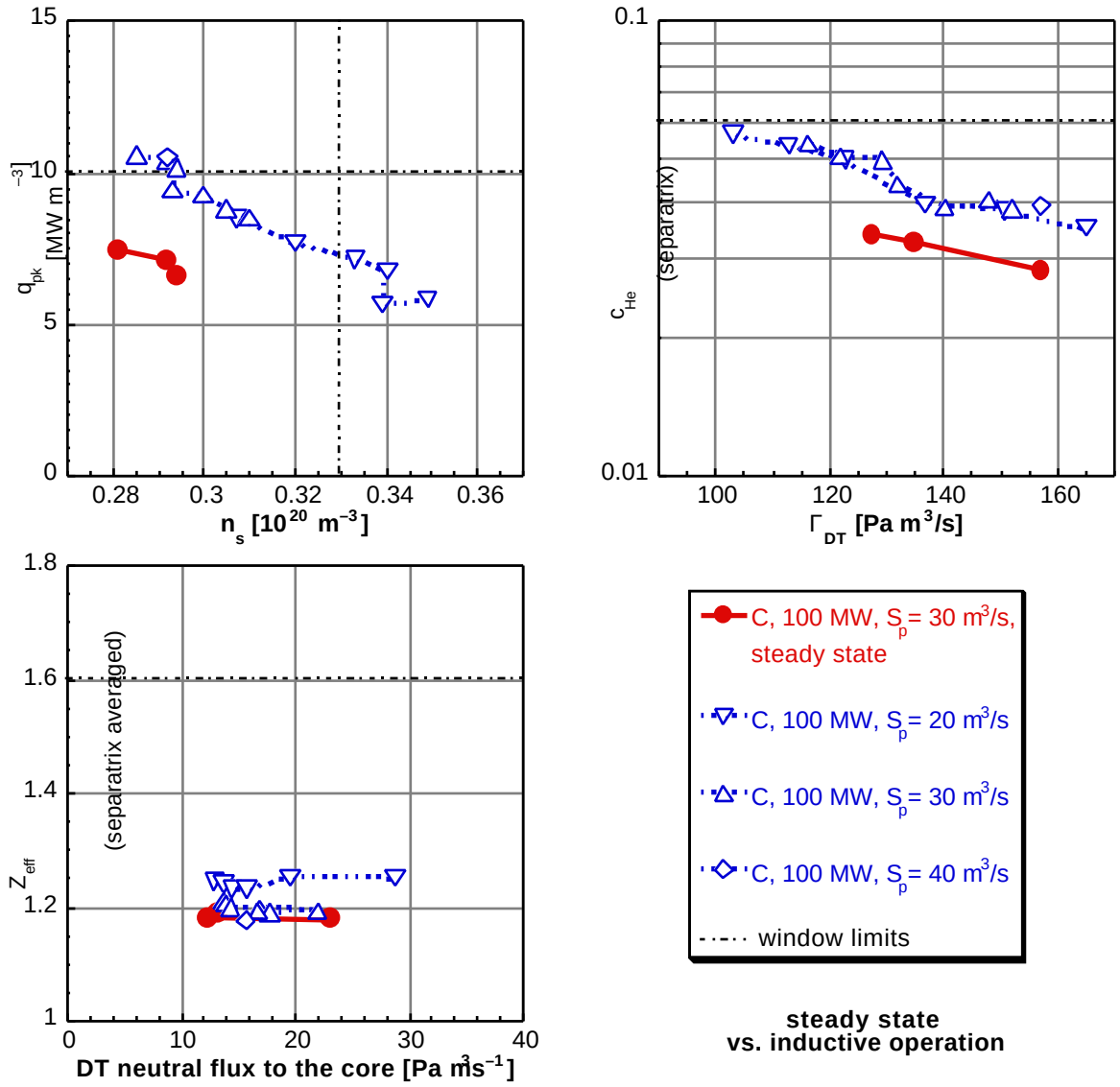

Figure 4.5.1-4 Three Views of the 6D Operational Window for the ITER Divertor for Steady State Operation with Carbon Target The data for inductive operation are also shown for comparison.

4.5.1.7 Conclusions

An acceptable operational window for the ITER divertor in inductive operation has been identified.

A V-shaped configuration of the target and divertor floor is beneficial for divertor performance, providing a considerable reduction of the peak power load on the target without adversely affecting helium removal. The effect is mostly due to accumulation of neutrals near the strike point when the V is plugged by plasma, as confirmed by the available experimental data from JET. However, such a configuration can negatively affect the operational flexibility of the machine by reducing the freedom of positioning the strike point. On balance, as a result of these studies, a V-shaped target configuration is foreseen for ITER.

Efficient particle exchange between the inner and outer divertors, via neutral gas in the private flux region, is essential to achieve an acceptable operational regime for the ITER divertor. The high gas throughput between the divertors, typically above 300 Pam^3/s, enhances the neutral-induced power dissipation in the outer divertor thus reducing the peak power load there. These results are consistent with JET experiments using the "septum" in the divertor, and the latest ITER divertor design takes them into account.

Impurity seeding can be used as an alternative to natural carbon radiation if the use of carbon were to become undesirable because of tritium co-deposition. Different radiating impurities can be used. In impurity seeding, the main trade-off is between the radiated power and Z_{eff} in the core, and the first results suggest that this trade-off is not strongly affected by the choice of impurity. The difference in fuel dilution, compared to C and among different seeded impurities, is also not large, unless the Z_{eff} is allowed to reach a value well above 2.

Further work is necessary to study the compatibility of acceptable divertor performance with steady state operation using non-inductive current drive in ITER, which requires an increase of the power entering the scrape-off layer and a decrease of the upstream plasma density. The first results suggest that the increase of the connection length caused by the reduction of the plasma current ensures lower peak power loading for the same upstream plasma density.

4.5.2 H-Mode Edge Pedestal and ELMs

4.5.2.1 H-Mode Edge Pedestal

In many tokamaks energy confinement during H mode strongly depends on the temperature at the top of the H-mode pedestal[1]. This pedestal temperature is determined by the pressure gradient and the width of the edge pedestal and the pedestal density. In the case of the Type-I ELMy regime, which is assumed for inductive operation in ITER, the pressure gradient is widely observed to be close to the ideal ballooning (first) stability limit. In DIII-D, the gradient is observed to be much steeper and it is suggested that the gradient is in the second stable region. However in this case the pedestal width is ~ half of the one in ASDEX-UP and thus the pressure on top of the pedestal is comparable between DIII-D and ASDEX-UP.

Experimental examinations of the pedestal width in individual machines[2], and also comparisons between two machines (C-MOD and DIII-D[3], JT-60U and DIII-D[4]) show that

[1] M. Greenwald, R.L Boivin, F. Bombard, et al., Nucl. Fusion **37** (1997) 793 W. Suttrop, F. Ryter, V. Mertens, et al., 17th IAEA Fusion Energy Conference, Yokohama, 1998, IAEA-F1-CN-69/EX2/06; G. Janeschitz, Yu. Igitkhanov, M. Sugihara, et al., 26 the EPS Conference on Contr. Fusion Plasma Physics, Maastricht, 1999, p1445

[2] A.E. Hubbard, R.L. Boivin, R.S. Granetz, et al., Phys. Plasmas **5** (1998) 1744; T.H. Osborne, K.H. Burrell, R.J. Groebner, et al., J. Nucl. Mat. **266-269** (1999) 131; R.J. Groebner, T.H. Osborne, Phys. Plasmas **5** (1998) 1800; J. Lingertat, V. Bhatnager, G.D. Conway, et al., J. Nucl. Mat. **266-269** (1999) 124; Y. Kamada, A. Isayama, T. Oikawa, et al., 17th IAEA Fusion Energy Conference, Yokohama, 1998, IAEA-F1-CN-69/CD2/EX9/2; W. Suttrop, M. Kaufmann, H.J. de Blank, et al., Plasma Phys. Control. Fusion **39** (1997) 2051

[3] R.S. Granetz, T.H. Osborne, R.L. Boivin, et al., 17th IAEA Fusion Energy Conference, Yokohama, 1998, IAEA-F1-CN-69/EX6/2

[4] T. Hatae, Y. Kamada, S. Ishida, et al., Plasma Phys. Control. Fusion **40** (1998) 1073

the pedestal width follows largely a thermal ion poloidal Larmor radius (ρ_{pol}) like dependence[1]. However, the actual pedestal width is several times wider than the poloidal Larmor radius and varies with the operational regime, e.g. is generally narrower in ELM free or in discharges in the second stability regime against ballooning than in ELMy discharges and is wider with a high z impurity injection in ELMy discharges than without the impurity injection[2].

A model for the pedestal width, which could partly explain these characteristics[3] is used to predict the pedestal width for ITER. It is based on turbulence suppression by the combined effects of the magnetic shear and the $\boldsymbol{E} \times \boldsymbol{B}$ shearing rate using the ITER pedestal database[4] for comparison to experimental data. The basic idea of the model is that the transport barrier is formed in the region where the turbulence is suppressed by a stabilizing $\boldsymbol{E}_r \times \boldsymbol{B}$ shearing rate, which is generated by the ion pressure gradient. The magnetic shear plays an essential role through two facts, namely that the critical pressure gradient at the ideal ballooning limit increases with increasing shear and that the turbulence growth rate decreases with increasing shear. The turbulence is completely suppressed when the $\boldsymbol{E}_r \times \boldsymbol{B}$ shearing rate is larger than the turbulence de-correlation rate[5] or its surrogate linear growth rate. The resulting expression of the pedestal width includes the toroidal Larmor radius and the magnetic shear. A plasma current dependence of the width appears indirectly through the magnetic shear, and thus the dependence becomes poloidal-Larmor-radius-like as observed on many machines. An approximately linear machine size dependence of the pedestal width appears through the magnetic shear profile.

Figure 4.5.2-1 shows a systematic density scan for type I ELMy discharges in JET with fixed toroidal field (2.3 T) and plasma current (2.5 MA) shown by closed squares. Also shown are predictions by several pedestal width models, namely a pure poloidal Larmor radius dependence (dashed), a constant pedestal width and thus pedestal pressure (dotted) as well as the above described ITER reference model (open circles). Predictions by the ITER model uses the magnetic shear calculated at the 95% flux surface by the EFIT code. Also the pedestal pressure in C-MOD can be reproduced as well by the ITER model as by the poloidal Larmor radius scaling. In addition, the observation that ELM free discharges and second stable discharges tend to show, in general, a smaller width than ELMy and first stable discharges, can be also reproduced by this model (shear changes with bootstrap current).

[1] M. Greenwald, R.L. Boivin, F. Bombard, et al., Nucl. Fusion **37** (1997) 793; W. Suttrop, F. Ryter, V. Mertens, et al., 17th IAEA Fusion Energy Conference, Yokohama, 1998, IAEA-F1-CN-69/EX2/06; G. Janeschitz, Yu. Igitkhanov, M. Sugihara, et al., 26 the EPS Conference on Contr. Fusion Plasma Physics, Maastricht, 1999, p1445 T.H. Osborne, K.H. Burrell, R.J. Groebner, et al., J. Nucl. Mat. **266-269** (1999) 131; R.J. Groebner, T.H. Osborne, Phys. Plasmas **5** (1998) 1800; J. Lingertat, V. Bhatnager, G.D. Conway, et al., J. Nucl. Mat. **266-269** (1999) 124; Y. Kamada, A. Isayama, T. Oikawa, et al., 17th IAEA Fusion Energy Conference, Yokohama, 1998, IAEA-F1-CN-69/CD2/EX9/2

[2] H. Kubo, S. Sakurai, N. Asakura, et al., Nucl. Fusion **41** (2001) 277.

[3] M. Sugihara, Yu. Igitkhanov, G. Janeschitz, et al., Nucl. Fusion **40** (2000) 1743

[4] M. Sugihara, Yu. Igitkhanov, G. Janeschitz, et al., 26th EPS Conference on Contr. Fusion Plas. Physics, Maastrich, 1999, p1449

[5] H. Biglari, et al., Phys. Fluids **B2** (1990) 1; T. Hahm and K. Burrell, Phys. Plasmas **2** (1995) 1648

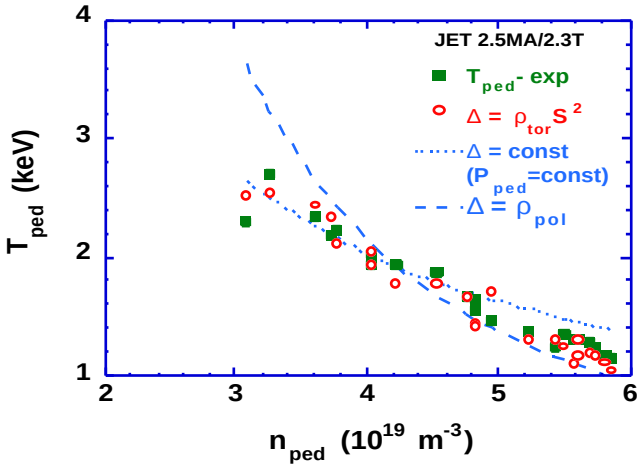

Figure 4.5.2-1 Pedestal Temperature T_{ped} vs. Pedestal Density n_{ped} for Type I ELMy Discharges in JET with Fixed Toroidal Field (2.3 T) and Plasma Current (2.5 MA) (closed squares)

Open circles are obtained from the width scaling with toroidal Larmor radius times shear squared (ITER model). Dashed and dotted lines are obtained from the width scaling based on poloidal Larmor radius and constant pedestal width, respectively.

Application of the above described reference model to ITER suggests that the expected pedestal pressure is (80-100) kPa. The pedestal density can be estimated by the experimental observation that the ratio of line average density and pedestal density is in the range of (0.7-0.9) for high density discharges close to the Greenwald density. Thus, for $\bar{n} \approx 10^{20} m^{-3}$ in ITER, $n_{ped} \approx (7-9) \times 10^{19} m^{-3}$ is expected. With this pedestal pressure and density, the expected pedestal temperature is $(3-4)\ keV$. The estimated pedestal temperature for ITER will be within the range where good confinement of the core plasma is maintained by ion temperature gradients. The expected range of pedestal values for ITER is summarised in Table 4.5.2-1.

Table 4.5.2-1 Reference Pedestal Parameters for ITER

Temperature T_{ped} (keV)	**Density** n_{ped} $(10^{19} m^{-3})$	**Energy** W_{ped} (MJ)	**Width** Δ_{ped} (cm)
3 - 4	7 - 9	100 - 120	10 - 15

This expected pedestal pressure (or pedestal energy) is also consistent with another observation of present day experiments, where the pedestal energy is approximately in the range of 1/3 of the total stored energy in good confinement H-mode discharges. Also, predictions based on non-linear offset type scaling laws used to extrapolate the pedestal energy to ITER provide similar values, albeit at present with a large uncertainty.

4.5.2.2 Energy Loss during Type I ELMs

The energy loss ΔW_{ELM} caused by Type I ELM is relatively large and can potentially produce significant erosion of the divertor target plates in a reactor like machine with high plasma energy content.[1]

Impact of the ELM energy deposition on the divertor plate due to sublimation (graphite) or melting (tungsten) can be characterised by $\Delta W_{ELM}/(S_{ELM}\sqrt{\delta_t})$ that is proportional to the surface temperature rise of the plate. Here S_{ELM} is the ELM energy deposition area and δt is the energy deposition time. Experimental database gives δ_t (0.1-0.2) ms in JET and JT-60U, δ_t (0.2-0.3) ms in DIII-D, and δ_t 0.4 ms or more in ASDEX Upgrade. Majority of the machines (JET, ASDEX Upgrade[2], JT-60U) observe that the ELM energy deposition area expands only slightly from the steady state heat deposition area S_{SS}, i.e., $S_{ELM} \equiv \zeta S_{SS} = (1\text{-}2)S_{SS}$ while $\zeta > 4$ in DIII-D[3]. IR measurements show that the energy deposition on the inner divertor plate is larger than the outer plate, although detailed specification is difficult due to the modified surface property by the deposited materials on the surface of the divertor plate. Radiation energy loss during the energy deposition is rather small, especially in the low to medium density discharges.

Critical values of deposited energy density, $E = \Delta W_{ELM}/S_{ELM}$, with which ITER divertor plate can withstand many numbers of ELM events, are calculated for CFC (2cm thick) and W (1cm thick) divertor plates for the expected range of deposition time δt = (0.1 - 1) ms. In the case of tungsten, melt limit is much stringent limitation than the evaporation limit. The critical values of the energy and flux densities for $\approx 10^6$ ELM during about 10^6 s burn with δt = (0.1 - 1) ms are (0.2 - 0.7) MJ/m^2 and (2 - 0.7) GW/m^2 in the case of CFC plate and (0.3 - 1) MJ/m^2 and (3 – 1) GW/m^2 in the case of W plate. In ITER, $S_{ELM} = 8\zeta$ m^2 and the critical energy is (1.6-5.6)ζ MJ for CFC and (2.4-8)ζ MJ for W with δ_t = (0.1 - 1) ms.

In several tokamaks, the ratio $\Delta W_{ELM}/W_{ped}$ has been investigated where W_{ped} is the pedestal stored energy. The ratio is 0.13 - 0.18 at low-to-moderate plasma density[4]. But the ratio is not constant and is strongly reduced in high density[5]. The ratio is well correlated with the pedestal collisoinality ν^* as shown in Figure 4.5.2-2.[6] Assuming that this collisionality dependence originates from the parallel ion transport process, the value of $\tau_{//} \quad 2L/c_s(1+\sqrt{3}/2\nu^*)$ relating to the parallel ion loss time (collisionless or collisional) would be the fundamental parameter (Figure 4.5.2-3).[7] Note that $\tau_{//}$ should include the transport time not only in the SOL region, but also in the ergodised (by an ELM) region

[1] ITER Physics Basis, Nucl. Fusion **39** (1999) 2430-2431
[2] A.W. Leonard, A. Herrmann, K. Itami, et al., J. Nucl. Materials **266-269** (1999) 109
[3] C.J. Lasnier, et al., 14th Int. Conf on Plasma Surface Interactions in Controlled Fusion Devices, May 22-26, 2000, Rosenheim, Germany, Report GA-A23399 to be published in J. Nucl. Mater
[4] A.W. Leonard, A. Herrmann, K. Itami, et al., J. Nucl. Materials **266-269** (1999) 109
[5] A. Mahdavi, et al., 18th IAEA Fusion Energy Conference, Sorrento, Italy (2000) IAEA-CN-77-EXP1/04
[6] A. Loarte, G. Saibene, R. Satori, et al., 18th IAEA Fusion Energy Conference, Sorrento, Italy (2000) IAEA-CN 77/ITERP/11(R)
[7] A. Loarte, G. Saibene, R. Satori, et al., 18th IAEA Fusion Energy Conference, Sorrento, Italy (2000) IAEA-CN 77/ITERP/11(R)

inside the separatrix. Both figures suggest $\Delta W_{ELM}/W_{ped} \geq 12\%$ or $\Delta W_{ELM} \geq 12$MJ for ITER in the case of $n_{ped} = 8x10^{19}\ m^{-3}$ and $T_{ped} = 3.5$ keV. If the expansion factor ζ is less than 2 and the ELM pulse length δ_t is much shorter than 1 ms, the estimated value of $\Delta W_{ELM} \geq 12$MJ will exceed the critical energy. The heat flux density is not clear from this study.

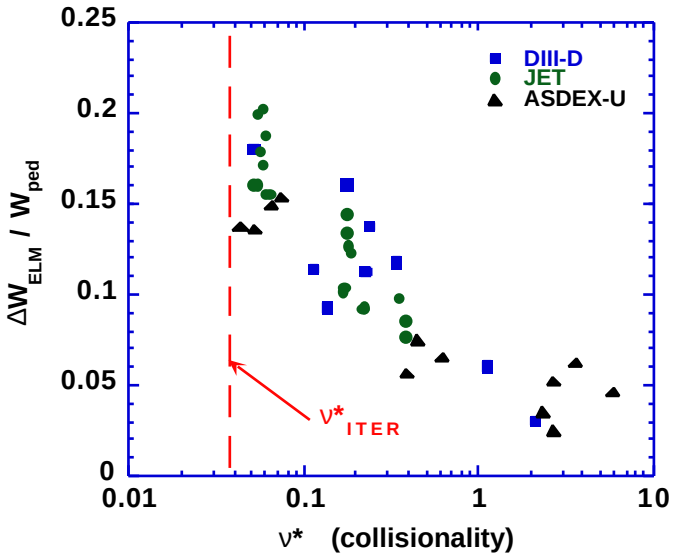

Figure 4.5.2-2 Energy Loss Fraction for ELMs as a Function of Pedestal Collisionality ν*

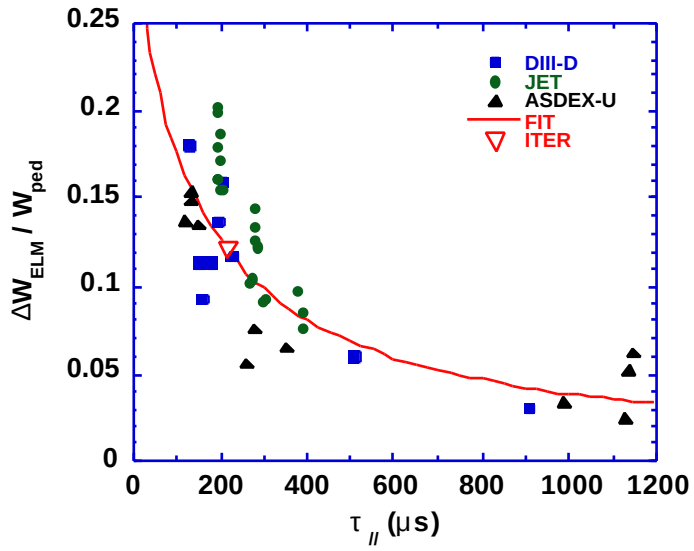

Figure 4.5.2-3 Energy Loss Fraction per ELM as a Function of Parallel Transport Time

The possible maximum heat flux density would be estimated from a sheath model by assuming pre-ELM pedestal density and temperature in the divertor region. The heat flux density on the divertor plate can be expressed as

$$q_{target} = \gamma k \Gamma_s T_s \sin\alpha, \qquad (4.5.2\text{-}1)$$

where γ is the heat transmission coefficient,[1]

$$\gamma = \frac{2.5T_i}{T_e} + \frac{2}{1-\delta_e} - 0.5\ln\left(2\pi\frac{m_e}{m_i}\left(1+\frac{T_i}{T_e}\frac{1}{(1-\delta_e)^2}\right)\right), \qquad (4.5.2\text{-}2)$$

δ_e is the secondary electron emission coefficient, $\Gamma_s = n_s c_s \approx 0.5 n_{div} c_s$ is the particle flux density along the field line (c_s is the sound velocity), and T_s is the electron temperature at the entrance of the sheath. The value of $\sin\alpha$ is evaluated from the magnetic equilibrium and divertor target geometry. This gives for ITER the upper limit of the heat flux density $q_{target} = 3.39$ GW/m^2 for the typical ITER conditions: $T_{ped} = 3.5$ keV, $n_{ped} = 8\text{x}10^{19}$ m^{-3}, and $\sin\alpha = 0.037$. It is assumed here that the incident ion energy at the sheath is $\approx 5T_{ped}$, the secondary electron emission[2] is ~ 0.2 giving $\gamma \sim 7.8$ for a DT plasma at $T_i = T_e$. This heat flux density would exceed the critical heat flux of (2-0.7) GW/m^2 for CFC and (3-1) GW/m^2 for W. It should be noted that the sheath model might overestimate the ELM energy loss.

A design solution exists for this problem: a tungsten target, inclined by a factor of two from the reference design, would withstand the type-I ELM heat load of most conservative estimation. The helium exhaust efficiency and heat load during steady state are tolerable. However, this design solution is associated with possible melting at disruptions and high particle recycling at upstream, i.e. some concern on the compatibility of H-mode confinement. Therefore the initial operation will use CFC as the target. The tungsten target may be used in the later stage after an experimental verification is made on ELM heat loads being unacceptable and control schemes are developed to reduce heat load during disruption to a tolerable level for tungsten.

Further studies are definitively needed to improve prediction of the divertor heat load associated with ELMs. In particular, the density scans for the ELM energy loss in various machines are particularly important for this purpose.

4.5.2.3 H-mode Regimes with Small ELMs

It is desirable to reduce the heat energy deposition to the divertor target due to ELM in order to increase the lifetime of the target. The pedestal energy can be reduced by reducing the pedestal density. This can be achieved with high-field-side pellet injection allowing, by density peaking, to reduce the pedestal density while maintaining the same temperature averaged density. The fast energy loss associated with the type I ELMs was reduced by a factor of 2 by pellet injection in experiment. Further studies should be performed in order to understand these possibilities and to study applicability of these methods to ITER.

Alternative high confinement modes with small ELM amplitude have been observed in most of divertor tokamaks, e.g., grassy ELMs in DIII-D[3], 'minute' ELMs in JT-60U[1], and the

[1] P.C. Stangeby, "The Plasma Boundary of Magnetic Fusion Devices" in Plasma Physics Series, Ed. P.Stott and H. Wilhelmsson, Institute of Physics Publishing, Bristol and Phyladelphia, 2000, p. 649
[2] K. Ertl, and R. Behrisch, "Electron emission from Solid Surfaces" in Physics of Plasma Wall Interactions in Controlled Fusion, Ed. D.E. Post and R. Behrisch, NATO ASI Series, Plenum Press, New York, 1986, pp. 515-538
[3] T. Ozeki, et al, Nucl. Fusion **30** (1990) 1425

enhanced D_α (EDA) mode in Alcator C-Mod[2] and recently in ASDEX-U[3]. Previously JET observed this mode as a so-called low particle confinement H-mode[4]. Although it is not yet verified that all these modes correspond to the same phenomenon, they are all classified as type II ELMs here for convenience.

Stability analyses and observations from DIII-D edge stability experiments[5] support an ideal stability based model of type I ELMs as low to intermediate toroidal mode number, n, kink-ballooning modes. In this model, second stability access plays a supporting role by facilitating the build-up of the edge pressure gradient and associated bootstrap current density, which then drives lower n MHD modes. The ELM amplitudes are assumed to be determined by the radial width of the unstable modes. Predictions from this model are consistent with many observed features of DIII-D edge stability experiments, as well as the observed increase of the edge pressure gradient with triangularity δ in DIII-D, JT-60U and ASDEX Upgrade.

In JT-60U, large amplitude low frequency ELMs (~100 Hz) are found to disappear and small high frequency grassy ELMs (~500-1000 Hz) to appear at sufficiently large δ ($\delta \geq 0.45$), q_{95} ($q_{95} \geq 6$) and β_p ($\beta_p \geq 1.6$).[6] At higher δ (0.54), type I ELMs can disappear at a lower q_{95} (~4). In the grassy ELMy H-mode, the peak heat load on the divertor plates is much smaller than that at type I ELMs. Edge stability analyses have revealed that the edge plasma is accessing to the second stability regime of high n ballooning modes in the grassy ELM discharges. Ideal stability analyses with careful equilibrium reconstruction including edge bootstrap current using EFIT[7] shows a possibility of intermediate n (= 5-10) modes as the trigger mechanism for type I ELMs and modes with $n \geq 10$ as the trigger for grassy ELMs. Modes with higher n are expected to be more localised due to shorter wavelength and will perturb a smaller edge region.

In the C-Mod EDA regime, periodic MHD relaxations are normally not observed.[8] The enhanced particle transport is caused by continuous, quasi-coherent density fluctuations which are localised in the density pedestal region. These have f~ 100 kHz in the laboratory frame and $k_\theta \sim 3\text{-}6\ cm^{-1}$. Perhaps because of their high k_θ, no magnetic signature has been observed so far. The 'low particle confinement' H-mode regime reported on JET[5] shares many characteristics of the EDA regime, but has not been as extensively studied or readily reproduced in their recent campaigns.

Most of the type II ELMy H-modes have similar pedestal parameters as type I ELMs and, thus, comparable energy confinement. The EDA mode like other 'small ELM' regimes, have the advantages of being steady state and avoiding impurity accumulation. The thermal energy

[1] Y. Kamada, et al, Plasma Phys. Control. Fusion **38** (1996) 1387
[2] M. Greenwald, et al, Plasma Phys. Control. Fusion **40** (2000) A263
[3] J. Stober, O. Gruber, A. Kallenbach, V. Mertens, F. Ryter, et al., Plasma Phys. Control. Fusion **42** (2000) A211
[4] M. Bures, D.J. Campbell, N. Gottardi, et al., Nucl. Fusion **32** (1992) 539
[5] J.R. Ferron, M.S. Chu, G.L. Jackson, et al., Phys. Plasmas **7** (2000) 1976
[6] Y. Kamada, et al., Plasma Phys. Control. Fusion **42** (2000) A247
[7] L.L. Lao, et al., Nucl. Fusion **41** (2001) 295
[8] M. Greenwald, et al, Plasma Phys. Control. Fusion **40** (2000) A263

confinement times agree well with type I ELMy H-mode.

The operating conditions required to attain regimes with small ELMs are now being investigated in many machines. It has been found that the most important parameters for obtaining such regimes are high triangularity and high safety factor. These operation conditions are summarised in Table 4.5.2-2.

Table 4.5.2-2 Summary of Operation Regime in Terms of q_{95} and δ for Grassy or EDA ELMs in Various Devices

Tokamak	Regime	δ_x	q_{95}
ASDEX-U[1]	Type II ELMy H-mode	≥ 0.4	≥ 4.2
C-MOD[2]	Enhanced D_α (EDA) H-mode	≥ 0.4	≥ 3.5
DIII-D	Type II or Grassy ELMy H-mode	≥ 0.4	
JET	Low Particle Confinement (LPC) H-mode		
JT-60U[3]	Grassy (minute) ELMy H-mode	≥ 0.4	≥ 4

The operational spaces for the grassy ELMs in JT-60 and EDA in C-Mod are similar. The similarity suggests that, despite the differences in observed edge phenomena, there may be similarities in the physics of the two regimes. Relatively high edge density and/or neutral pressure also appear to play a role in accessing the EDA mode on C-Mod. In ASDEX Upgrade, type I ELMs gradually decrease from the mixture of type I and II ELMs with increasing density and pure type II ELMs appear at relatively high density ($\bar{n}/n_G > 0.8$). For higher density ($\bar{n}/n_G > 0.95$), the discharge suffers of a sharp transition to type III ELMs, which leads to reduced confinement. Small ELMs have been observed in various machines with ohmic, ICRF and NB heating, showing that they are not related to heating method or fast particles. There does not seem to be a clear power threshold, as long as the power outflow through the separatrix is sufficient to avoid type III ELMs.

According to the present database, the type II ELM regime requires higher q_{95}, and thus lower plasma current, than the type I ELM regime thus leading generally to a reduced confinement time. The amount of plasma current reduction required for achieving the type II ELM regime is uncertain and might be somewhat mitigated when a second separatrix is very close to the first one at higher triangularity (higher shear). Type II ELM regime could be also used for hybrid or steady state operations with higher q. Further systematic experimental studies in existing machines should be performed more extensively to extend this ELM regime even into the reference operation mode of ITER.

Another possible way to improve confinement in regimes with reduced ELMs is creating a peaked density profile by pellet injection. Pedestal pressure can be reduced to the extent, where the associated confinement degradation can be compensated by the density profile

[1] F. Ryter, J. Stober, A. Stäbler, et al., 18th IAEA Fusion Energy Conference, Sorrento, Italy (2000) IAEA-CN 77/EX2/2
[2] M. Greenwald, et al, Phys. Plasmas **6** (1999) 1943
[3] Y. Kamada, et al, Plasma Phys. Control, Fusion **40** (2000) A247-A253

peaking. This has been demonstrated by the high field side (HFS) pellet injection in ASDEX Upgrade.[1] Essential point of this mode of operation is the pellet penetration depth and the resultant profile peaking. Although the HFS pellet injection is planned in ITER for this purpose, the effectiveness still needs to be confirmed in large machine with high pedestal pressure.

Improved confinement due to the density profile peaking has also been observed in RI mode.[2] In this case, the profile peaking is produced spontaneously with impurity puffing. In TEXTOR, with neon seeding,[2] the H_{H93} factor larger than 1.2 has been achieved and sustained for about $100\tau_E$ in discharges with L-mode edge at 1.2 times the Greenwald density. Confinement improvement in experiments with impurity injection was observed also in DIII-D,[3] JET[4] and JT-60U[5] (see also Section 2.2.2 and Annex A2.2.3). Further systematic studies of RI-mode in large machines are needed for extrapolation of this mode to ITER conditions (e.g. in JT-60U with 16-20 MW of heating power).

4.6 Energetic Particle Confinement

In ITER plasmas, a variety of suprathermal ions will be produced by NB injection, ICH&CD and fusion reactions. Good confinement of energetic alpha particles produced by fusion reactions is essential for attaining and sustaining high Q operation in ITER. It is expected that the energetic ion behaviour will be close to classical in a quiescent plasma, based on the present experimental results with additional heating in large tokamaks.

Different loss channels have been analysed in order to develop the design specification and requirements. The major potential loss channels for energetic particles in ITER are TF ripple and the effect of collective instabilities including those excited by energetic particles such as TAE (toroidal Alfven eigenmode) and fishbone instability.

4.6.1 Ripple Loss of Energetic Ions

Potentially significant loss of fusion alpha particles and high-energy ions produced by NB injection or ICH&CD can occur in ITER due to toroidal field (TF) ripple, i.e. perturbations of the toroidal magnetic field due to discreteness of the TF coils[6]. The TF ripple amplitude is defined as

$$\delta(R,Z) = \frac{B_{max} - B_{min}}{B_{max} + B_{min}} \qquad (4.6.1\text{-}1)$$

where B_{max} and B_{min} are maximum and minimum magnetic field strengths at a circular line with given (R, Z). Without Ferromagnetic Inserts (FI) the maximum ripple amplitude at the

[1] P.T. Lang, J. Gafert, O. Gruber, et al., Nucl. Fusion **40** (2000) 245
[2] A.M. Messian, et al., Nucl. Fusion **34** (1994) 825
[3] M. Murakami, et al., Nucl. Fusion **41** (2001) 317
[4] G.P. Maddison, et al., 18th IAEA Fusion Energy Conf., Sorrento, Italy (2000) IAEA-CN-77/EX5/4
[5] H. Kubo, et al., 18th IAEA Fusion Energy Conf., Sorrento, Italy (2000) IAEA-CN-77/EX5/3
[6] ITER Physics Basis, Chapter 5 Section 3, Nucl. Fusion **39** (1999) 2475-2478

plasma separatrix in ITER is 1.3%. An essential reduction of ripple amplitude can be achieved using ferromagnetic inserts[1]. At the nominal value of toroidal field, the planned configuration of the FI set[2] provides a reduction of the ripple amplitude by a factor of 1.5 at the separatrix and is even more effective in the inner plasma regions.

Alpha particle loss rates have been calculated for the nominal Q = 10 inductive and two reverse shear (RS) steady-state operating scenarios using the HYBRID Monte-Carlo numerical code.[3] Results are shown in Table 4.6.1-1 for the cases with and without FI. In the absence of FI, the particle and power losses in the inductive regime as well as in the steady-state regime with a weak RS ($q_{min} \approx 2$) are tolerable. In the scenario with a strong RS ($q_{min} \approx 3.75$), α-particle losses in the absence of FI are rather large. The peak power load on the first wall produced by the escaping α-particles in this scenario exceeds the wanted level of 0.5 MW/m^2. Ripple losses of fast ions produced by NB injection are also rather large in this case (Table 4.6.1-2). In the presence of FI the ripple losses of alpha particle and NB ions become negligible in the ITER inductive scenarios and are reduced to values well below the permissible level in the reverse shear steady-state scenarios.

Table 4.6.1-1 Ripple Loss of Fusion Alpha Particles in Various ITER Scenarios With and Without Ferromagnetic Inserts (FI)

	Inductive		Weak RS (#4)		Strong RS	
	No FI	With FI	No FI	With FI	No FI	With FI
Total particle loss fraction (%)	2.15	negligible	6.5	0.08	21	0.75
Total power loss fraction (%)	0.65	negligible	2.5	0.04	9.3	0.13
Peak FW heat load (MWm^{-2})	< 0.1	negligible	0.23	0.005	0.8	0.025
Plasma current (MA)	15		10		10	

Table 4.6.1-2 NB Ion Ripple Loss with and without Ferromagnetic Inserts in Configuration with Strong Reversed Shear for Off-axis NB Injection

	No FI	With FI
Particle loss fraction	15.5%	0.5%
Power loss fraction	3.2%	0.05%
Maximum heat load at P_{NB}=50 MW	230 kWm^{-2}	< 10 kWm^{-2}
Plasma current (MA)	10	10

In ITER plasmas, the reversal of the ion [**B**× B] drift direction weakly affects the α-particle and NB ion ripple loss. Counter (to the plasma current) NB injection will be accompanied by an appearance of prompt (first orbit) losses. These losses could be substantial due to a high density at the plasma periphery where a significant fraction of the beam atoms will be ionized
.

[1] H. Kawashima, et al., 18th IAEA Fusion Energy Conference, Sorrento, Italy (2000) IAEA-CN-77/EX9/3
[2] A. Alekseev, E. Lamzin, et al., "Calculation of Ripple in the ITER Facility", Final Report, Efremov ITER Design Office, July 2000
[3] S. Konovalov, T. Takizuka, K. Tani, K. Hamamatsu, and M. Azumi, JAERI-Research 94-033, 1994

4.6.2 Fast Ion Instabilities

A variety of collective instabilities with a wide range in frequency may be driven by energetic particles including alpha particles. Results from present day experiments have shown that two classes of instabilities are effective in causing anomalous transport of energetic ions: 1) high frequency instabilities such as the shear Alfven eigenmodes and 2) lower frequency instabilities such as the fishbones associated with the toroidal precession of trapped fast particles.

4.6.2.1 Alfven Frequency Modes

Toroidicity causes the continuous frequency spectrum of shear Alfven waves in a tokamak plasma to exhibit a radial "gap". Within this gap the discrete frequency modes called toroidal Alfven eigenmodes (TAE) can exist. The frequency gap is centred at

$$\Omega_{TAE}(r_0) = v_A k_{//} = v_A/(2qR) \qquad (4.6.2\text{-}1)$$

with v_A the Alfven speed, q the safety factor at the gap location, and R the major radius. The relative gap width of the frequency is of the order of inverse aspect ratio. Since alpha particles in thermonuclear plasma have velocities that are typically super-Alfvenic, they can resonantly interact with weakly damped TAE modes and destabilise them.

Various forms of Alfven eigenmodes exist in a toroidal plasma which can be spontaneously excited by energetic alpha particles. These modes present a potential danger to fusion reactors, because they can eject high energy alpha particles from the plasma before their thermalisation. Since they can carry considerable energy, these losses may damage the first wall of reactors.

During the past years, the close interaction between theory and experiment has led to many discoveries on Alfven eigenmodes in toroidal plasmas. Most of data come from experiments with neutral beams and ICRF heating. A great deal of theoretical work have been carried out on energetic particle pressure gradient drive and competing damping mechanisms for both thermal and fast ions, electron Landau damping and trapped electron collisional damping.

Recently detailed comparisons have been carried out in conventional JET discharges, showing a quantitative agreement between first principle gyrokinetic calculations and measurements of Alfven eigenmode damping rates.[1] They provide the theory required to make extrapolations for a reactor, since the thermonuclear conditions with a significant alpha-particle power cannot be accessed with similarity experiments and dimensional scalings based on the results from tokamaks that are now in operation.

The results of calculations with the global gyrokinetic PENN code predict that conventional burn scenarios, with monotonic safety factor around unity in the plasma core, exist where all the AEs of global character with low to intermediate n (= 1–12) are stable.[2]

[1] A. Jaun, et al., Phys. Plasmas **5** (1998) 2952; A. Fasoli, et al., Phys. Lett. **A265** (2000) 288
[2] A. Jaun, et al., Nucl. Fusion **39** 11Y (1999) 2095

Calculations using the MISHKA1 code have shown that high-n ($17 \leq n \leq 26$) AEs are stable at (flattened) post-sawtooth β_α profiles in the ITER-98 ignited scenario but unstable at peaked pre-sawtooth profiles.[1] Analysis of the nonlinear evolution of unstable spectrum of these modes, restricted to the radial domain $0.2 \leq r/a \leq 0.4$, in a simplified circular geometry under otherwise ITER-like conditions, indicates that such group of modes leads to rather insignificant anomalous alpha-particle redistribution even in worse than expected conditions. The possibility of significant redistribution via interaction with more radially extended modes remains to be clarified.

Modelling of the drift kinetic Alfen eigenmodes (DKAEs) using the PENN code has revealed[2] a strongly unstable n=3 mode in ITER like plasma with a deeply reversed magnetic shear (I = 8 MA, q(0)=4.5, $q_{min} = 3.77$) and $\omega_{*,bulk}/\omega_{TAE} \approx 0.01n$. The theoretical understanding of DKAE instabilities is however still limited. With the present knowledge, it is advisable to avoid scenarios where the ratio $\omega_{*,bulk}/\omega_{TAE}$ exceeds $\approx 0.002n$, in order to remain in a regime where little degradation of fast particle confinement has been observed experimentally in JET.

It is therefore desirable to develop advanced tokamak burn scenarios with a flat or weakly inverted safety factor ranging between $q \approx 1 - 2$ in the core.

4.6.2.2 Fishbone Instability

The fishbone instability is the resonant wave-particle interaction between the toroidal precession of trapped energetic particles and the toroidal wave velocity of m = 1, n = 1 MHD perturbations. Fusion alpha particles typically have energies such that their magnetic precession frequency $\omega = E_\alpha/(ZeBRr)$ is much higher than the thermal ion diamagnetic precession frequency. In this case, the threshold for the excitation of alpha-driven precessional drift fishbones depends on the alpha particle β. An analytic study including the effects of shaping, finite aspect ratio and finite beta, found fishbone instability occurred when the alpha particle β exceeds 1% on axis. As this is only slightly higher than the normal value expected in ITER, alpha-particle-driven fishbone oscillations may actually occur. However, according to calculations of anomalous transport of alpha particles due to fishbones, although redistribution of the alpha particle profile is caused, loss of trapped alpha is not expected.[3]

4.7 Conclusions

The physics analysis outlined in this chapter demonstrates that ITER satisfies its objectives: inductively-driven DT discharge with Q > 10 lasting for 300-500 s with sound margins in confinement, β and L-H transition power. The nominal operation density is 85% of the Greenwald density, which enables operation with high reliability, particularly with high plasma triangularity. Recent results from JET and ASDEX-Upgrade have given confidence on maintaining $H_{H98(y,2)} \sim 1$ at $n \sim n_G$. Even with $I_p = 15$ MA and $H_{H98(y,2)} = 1.0$, operation with

[1] J. Candy, et al., Phys. Plasmas **4** (1997) 2597
[2] A. Jaun, et al., Nucl. Fusion **40** (2000) 1343
[3] ITER Physics Basis, Chapter 5 Section 4, Nucl. Fusion **39** (1999) 2478

reduced additional heating with $n = n_G$ would enable achievement of $Q \sim 20$. High current (e.g. 17 MA) operation will enable studies on plasmas with high $Q \sim 50$, i.e. plasmas which are almost fully self-sustained. Improved confinement by a factor of 1.2 or improved confinement up to the Greenwald density would also allow sub-ignition studies at 15 MA.

The operational scenarios that are under consideration for steady-state operation involve modest (currents ~ 9 MA) with negative shear. However, modest current, steady-state operation requires challenging values of confinement improvement ($H_{H98(y,2)} \sim 1.5$) and β ($\beta_N \sim 2.7$). Although these values have been obtained in recent experiments, further investigation will be required to establish the operation scenarios: pressure and current profile control, stability control, and divertor compatibility. Hybrid operation, with combined inductive and non-inductive current drive, will provide long pulses (e.g. > 1,000 s) with a more modest requirement on confinement ($H_{H98(y,2)} \leq 1.0$). This scenario offers a candidate operation mode for material tests.

ITER has the capability to exploit NB, EC, IC and/or LH for heating and current drive, which, taking advantage of their different characteristics, offers flexibility and variation in experimental operation. In addition, the diagnostics system is designed to satisfy the profile control needs of enhanced modes of operation.

The advanced features of ITER include ECCD for stabilising neoclassical tearing modes, saddle coils external to the toroidal field coils for stabilising resistive wall modes, and high-field-side pellet injection, all of which will expand the operational space and/or improve the stability characteristics of discharges with high β and high density.

The reference operation at $q_{95} \sim 3.0$ is associated with large uncertainty in projecting the ELM heat load onto the divertor targets. All available models lead to values of the energy density on the divertor target larger than what would be permitted to achieve an acceptable target lifetime due to erosion. Even if the most conservative value based on sheath-limited power transfer to the target is not too much larger than the acceptable value (less than 2), it is important to consider a number of alternative scenarios to be used to reduce the ELM amplitude. A design solution exists for this problem: a tungsten target, inclined by a factor of two from the reference design, would withstand the type-I ELM heat load of most conservative estimation. The helium exhaust efficiency and heat load during steady state are tolerable. However, this design solution is associated with possible melting at disruptions and high particle recycling at upstream, i.e. some concern on the compatibility of H-mode confinement. Therefore the initial operation will use CFC as the reference target. The tungsten target may be used in the later stage after an experimental verification is made on ELM heat loads being unacceptable and control schemes are developed to reduce heat load during disruption to a tolerable level for tungsten. High density or density peaking by pellet injection and ion heating by IC H&CD would facilitate reaching $Q \geq 10$ at 13 MA ($q_{95} \sim 3.5$), where more benign ELMs are expected (type II ELM regime). Furthermore, weak-negative-shear operation would provide a scenario for reaching $Q \geq 10$ at $q_{95} \sim 4$.

To summarise, the physics design concept of ITER satisfies the stated mission, embodies all the state-of-the-art tokamak physics knowledge available to date, and is compatible with the

constraints of engineering and cost. ITER will allow, for the first time, plasma physics studies on confinement, MHD stability, divertor, and energetic particle confinement, under completely integrated, reactor-relevant conditions, and for pulse lengths significantly longer than the characteristic times of plasma processes. Also, its flexibility in fusion power, plasma density, beta, shaping, heating and current drive methods, fuelling, and replaceable in-vessel components, will accommodate uncertainty in projection, and facilitate the investigation and optimisation of burning plasma. Furthermore, significant α heating, high β, large size and long burn, are expected to define and optimise operation regimes attractive for a reactor as well as new aspects of plasma physics. ITER, with its extensive diagnostics and considerable flexibility, is an essential and powerful vehicle for the exploration of these frontiers.